Doctoral Thesis

Pathological mechanisms in Crohn's disease via dysbiosis triggered by Paneth cell α-defensin misfolding

（Paneth 細胞α-defensin の misfolding に起因する dysbiosis を介したクローン病の病態形成メカニズム）

Yu Shimizu

Innate Immunity Laboratory

Transdisciplinary Life Science Course

Graduate School of Life Science

Hokkaido University

2020. 12

Contents

1. Introduction

In the human intestinal tract, forty trillion of commensal bacteria construct complex ecosystem termed intestinal microbiota[1]. The human intestinal microbiota is thought to possess approximately 10 million genes which are more than several hundred times larger than that of the host[2], and involved in many aspects of host physiology, that includes energy metabolism[3], immune system regulation[4], and nervous system development[5]. Recently, associations with imbalance of the intestinal microbiota, termed dysbiosis, and many diseases, including chronic lifestyle diseases such as obesity and diabetes, immunological disorders, and nervous system diseases have been reported[6]. α-Defensin, a major family of mammalian antimicrobial peptides, are known regulators of the intestinal microbiota. These ~ 4 kDa, basic peptides are characterized by evolutionally conserved Cys residue positions that are invariantly spaced to form disulfide bonds between Cys^{I}-Cys^{VI}, Cys^{II}-Cys^{IV}, and Cys^{III}-Cys^{V} [7]. In the intestinal epithelium, α-defensin occur only in intracellular dense-core secretory granules of Paneth cells, one of the major terminally differentiated lineages of the small intestine. Paneth cells, which reside at the base of the crypts of Lieberkühn, release secretory granules that are rich in α-defensin, termed cryptdins (Crps) in mice and HD5 and HD6 in human, in response to bacteria and other stimuli at effective concentrations, thereby contributing to enteric innate immunity[8–13]. Also, Paneth cell α-defensin contribute to regulating the composition of the intestinal microbiota in an activity-dependent manner *in vivo* as well as affecting development of host adaptive

immunity[14]. Furthermore, oral administration of Crp4 prevents severe dysbiosis in mouse graft-versus-host disease[15,16], indicating that Paneth cell α-defensin secreted into the intestinal lumen contribute not only to innate immunity but also to maintenance of intestinal homeostasis by regulating the intestinal microbiota[17,18].

Recently, a relationship has been revealed between the intestinal microbiota and the pathophysiology of Crohn's disease (CD)[19]. CD is a chronic inflammatory bowel disease that may affect the entire gastrointestinal tract, especially the terminal ileum, with chronic inflammation and ulceration[20]. The number of patients with CD has been increasing continuously worldwide, including Europe, The Americas and Asia[20–22]. Because CD typically appears in younger people in their teens and 20s and any radical treatments have yet to be developed, the patient's quality of life could be diminished for a lifetime. Although a complete picture of CD pathogenesis is lacking, there is consensus that dysbiosis and dysregulated immune responses to the intestinal microbiota play important roles[20]. Moreover, both genetic factors consisting of more than 160 susceptibility loci[23], as well as environmental factors such as overuse of antibiotics[24] and adoption of "westernized diets"[25] have been reported as CD risk factors, and these factors are suggested to induce pathophysiology of CD via dysbiosis[26].

Evidence shows that certain Paneth cell defects are involved in CD onset and pathophysiology. Paneth cells continuously synthesize high levels of secretory proteins in the

endoplasmic reticulum (ER) and are susceptible to ER stress, a failure of maintaining ER homeostasis induced by accumulation of misfolded proteins[27]. Excessive ER stress induces series of signal cascades termed unfolded protein response (UPR), and UPR manages to recover ER homeostasis by inducing suppression of protein translation, induction of ER chaperones which help refolding of the misfolded proteins, and degradation of the misfolded proteins via autophagy and activation of ubiquitin-proteasome system[28]. Several genes involved in resolution of ER stress affect CD susceptibility, and deletions or mutations of such gene. For example, UPR-related genes *XBP1*[29] and *AGR2*[30], autophagy-related genes *ATG16L1*[31], *IRGM1*[32], and *LRRK2*[33] cause Paneth cell abnormalities in granule morphology and cellular localization in mouse models. In CD patients with mutations in *XBP1*[29] and *ATG16L1*[31], Paneth cell abnormalities occur which are similar to those observed in genetically deficient mice. Moreover, several studies have identified relationships between ER stress in Paneth cells and disruptions of the intestinal microbiota in CD. The appearance rate of Paneth cells with abnormal granule morphology in CD patients is associated with dysbiosis that is characterized by reduction of diversity and decrease of anti-inflammatory bacteria such as *Faecalibacterium*[34]. CD patients positive for the ER stress marker GRP78 in Paneth cells harbor greater numbers of CD associated enteroinvasive *Escherichia coli* compared to patients that lack GPR78-positive Paneth cells[35]. Although these findings suggest the involvement of ER stress, Paneth cell dysfunction, and dysbiosis in CD pathophysiology, causal relationships between these factors remain to be

demonstrated.

Excessive ER stress induces abnormal post-translational modifications in proteins including the misfolding of disulfide bonds[36,37]. It is known that formation of tertiary structure of proteins by disulfide bond formation has important roles in regulating function and stability of the proteins[38]. For example, oxidized-form Crps (oxCrps) containing three intramolecular disulfide bonds elicit strong bactericidal activities against pathogenic bacteria and minimal or no bactericidal activities against commensal bacteria *in vitro*. In contrast, disulfide-null reduced-form Crps (rCrps) kill both pathogens and commensals *in vitro*[39]. Furthermore, CD patients have reduced-form HD5 in their ileal tissue, a condition not detected in healthy subjects[40]. Taken together, It was hypothesized that excessive ER stress in Paneth cells would promote biosynthesis of reduced-form α-defensin due to disulfide bond misfolding and that secretion of reduced-form α-defensin into the intestinal lumen would disrupt the spectrum of bactericidal activities against commensals and induce dysbiosis, resulting in the onset of CD pathophysiology. However, whether ER stress in Paneth cells induces α-defensin misfolding, and whether reduced-form α-defensin are secreted into the intestinal lumen and further cause dysbiosis *in vivo* have been completely unknown.

Therefore, this study aims to clarify relationships among α-defensin misfolding, ER stress in Paneth cells, and CD pathogenesis via the intestinal microbiota by using SAMP1/YitFc, a murine model known to develop CD-like ileitis spontaneously[41–43].

2. Methods

Mice

SAMP1/YitFc mice were obtained from Charles River Laboratory Japan Inc. and propagated at Hokkaido University. ICR mice were obtained from CLEA Japan Inc. at 3 w. All mice were raised under conventional conditions maintained under a 12 h light/dark cycle with water and food provided *ad libitum*. All animal experiments in this study were approved by the Institutional Animal Care and Use Committee of the National University Corporation at Hokkaido University, and conducted in accordance with Hokkaido University Regulations of Animal Experimentation.

Histological analysis

Mice were euthanized by isoflurane inhalation and all efforts were made to minimize suffering. Then, ileum (distal one-third of the small intestine) was opened, washed for removing debris with ice-cold PBS (-), and rolled longitudinally into a Swiss-roll configuration. Ileal tissues were fixed in 10% buffered formalin, embedded in paraffin, and sliced into 4 μm sections. Deparaffinized sections were stained with Hematoxylin-Eosin (HE) and Alcian blue. For histological evaluation, 1 through 10 well-orientated crypt-villus axes showing complete longitudinal sectioning were sequentially selected from each HE section from the distal end. Each crypt-villus axis was evaluated following 3 categories: [a]

inflammatory infiltration (the number of inflammatory cells in the lamina propria), [b] villus distortion (ratio of villus length to crypt depth) and [c] thickening of muscle layer (thickness of muscle layer directly under the crypt). To determine the range for scoring in [a]–[c], all sections obtained from each ICR and SAMP1/YitFc mouse were pre-examined. In [a] and [c], mean + 2 standard deviation (SD) of measured values in ICR mice was set as the upper limit of score = 0. Then, the range between mean + 2SD in ICR mice and maximum value in SAMP1/YitFc mice was divided into three equal parts, and each part was set as the range of score 1, 2, and 3. In [b], mean - 0.5 of measured values in ICR mice was set as the upper limit of score = 0. Then, the range between mean -0.5 in ICR mice and minimum value in SAMP1/YitFc mice was divided into three equal parts, and each part was set as the range of score 1, 2, and 3. In scores of [d] crypt abscess in each mouse were calculated by multiplying 0.5 and the number of crypt abscesses in the entire area of the sections together based on a previous study[44]. Established criteria were listed in Table 1. Under these criteria, over 90% of ICR mice were scored to 0. Then, each crypt-villus axis was graded from 0 to 3 in each category based on the criteria. Scores of [a]–[c] for each mouse were calculated as averages of crypt-villus axes evaluated in the sections. Total inflammatory score of each mouse was calculated by a summation of [a]–[d].

Immunohistochemistry

Deparaffinized ileal sections were rehydrated, and antigen retrieval was conducted by boiling in pH

9.0 solution (Nichirei bioscience) at 105ºC for 20 min. Sections were covered by blocking solution containing 20% Block ace (Dainippon Pharmaceutical) in PBS supplemented with 5% goat serum (Sigma-Aldrich) and incubated at room temperature for 30 min. After blocking, sections were reacted with primary antibodies: anti-Muc2 (1 μg/mL, sc-15334, Santa Cruz Biotechnology), anti-Crp1 (1 μg/mL, 77-R63, self-produced), anti-GRP78 (1 μg/mL, ab21685, Abcam), anti-calreticulin (10 μg/mL, #62304, Cell Signaling), anti-Ephrin-B2 (10 μg/mL, AF496, R&D systems), and anti-MIST-1 (0.25 μg/mL, ab187978, Abcam) at 4ºC for overnight. After washing, sections were reacted with fluorescent-conjugated secondary antibodies (Life technologies) at room temperature for 1 h. After the reaction, sections were covered with coverslips mounted with VECTORSHIELD medium with DAPI (Vector Laboratories), sealed with nail polish and dried. Then, fluorescence images were observed using confocal microscopy (LSM510, Carl Zeiss A1, Nikon).

Transmission electron microscopy

5 mm-long segments of terminal ileum were fixed by 2% paraformaldehyde and 2% glutaraldehyde at 4°C overnight, post-fixed with 2% osmium tetroxide at 4°C for 2 h, dehydrated and embedded in Quetol-812 epoxy resin (Nisshin EM). Then, fixed tissues were cut into 70 nm ultrathin sections using Ultracut UCT (Leica Microsystems). The sections were mounted on copper grids, and then stained with 2% uranyl acetate at room temperature for 15 min followed by staining with Lead stain solution

(Sigma-Aldrich). Images were obtained by JEM-1400Plus transmission electron microscope (JEOL Ltd.) at an acceleration voltage of 100 kV. For quantitative analysis of secretory granules, all granules in randomly selected Paneth cells were measured. For quantitative analysis of ER lumen diameter, 5 ER cisternae were sequentially selected from the closest to nuclei of each selected Paneth cell, then the length of most expanded part of each ER cisterna was measured and averaged as ER lumen diameter of each Paneth cell. All measurements were conducted by using ImageJ software (National Institutes of Health, http://rsb.info.nih.gov/ij/).

Crypt isolation

Crypt isolation and fractionation were conducted by previously described method[45] by using 5 cm of terminal ileum tissues. The fraction with > 70% purity of crypts was used in this study.

SDS-PAGE western blot

Proteins were extracted from Isolated ileal crypts by lysing in RIPA buffer (50 mM Tris-HCl pH 8.0, 150 mM NaCl, 0.1% Triton-X 100, 0.1% SDS), and then protein content of sample were measured by using the BSA Protein Assay Kit (Thermo Fisher Scientific) following the manufacturer's protocol. Proteins extracted from each crypt samples were adjusted to 20 μg of protein extracted and were dissolved in tricine sample buffer (BIO-RAD), and then analyzed by SDS-PAGE using Mini-

PROTEAN TGX Precast gels (BIO-RAD). After electrophoresis, proteins were transferred to 0.22 μm PVDF membrane at 1.3 V for 7 min using Trans-Blot Turbo Transfer system (BIO-RAD). After transfer, membranes were incubated with blocking buffer containing 5% BSA (Sigma-Aldrich) in 0.1% TBS-T at 4ºC for overnight and then reacted with following primary antibodies: anti-ATF4 (1/1,000, #11815, Cell Signaling), anti-phospho-IRE1α (1 μg/mL, NB100-2323, Novus Biologicals), anti-total IRE1α (1 μg/mL, NB100-2324, Novus Biologicals), anti-ATF6 (1 μg/mL, NBP1-40256, Novus Biologicals), anti-GRP78 (1/1,000, #3177, Cell Signaling), and anti-HPRT1 (0.018 μg/mL, ab109021, Abcam) at 4ºC overnight. After washing with 0.1% TBS-T, membranes were incubated with HRP-conjugated secondary antibodies (GE Healthcare) at room temperature for 1 h and visualized by Chemi-Lumi One Ultra (Nacalai Tesque). For the quantification of each molecule, band intensities were determined by ImageJ software.

Dot blot analysis

50 ng of chemically synthesized Crps were dissolved in 5% acetic acid and pipetted onto a 0.1 μm nitrocellulose membrane (GE Healthcare). Peptides were immobilized on the membrane by drying. After drying, the membrane was treated as described for AU-PAGE western blot.

Protein purification from small intestinal tissue

Full length of small intestinal tissue was obtained from ten ICR and ten SAMP1/YitFc mice and luminal debris were rinsed by ice-cold PBS (-). Tissue samples were minced in ice-cold PBS (-) supplemented with 100 mM iodoacetamide (Nacalai Tesque) and Complete Mini protease inhibitor cocktail (Roche Applied Science). Then, the tissues were completely homogenized using a Potter homogenizer and rotor-stator homogenizer TissueRuptor (Qiagen). For alkylation reactions, homogenized samples were incubated at room temperature for 1 h under shading. After the reaction, acetic acid (Nacalai tesque) was added to a final concentration of 30% (v/v) and rotated at 4ºC for overnight. Precipitates were removed from homogenized samples by centrifugation (15,000 g for 30 min) at 4ºC. Supernatants were dialyzed using SpectraPor7 membranes (Spectrum Labs) against 5% (v/v) acetic acid at 4ºC and concentrated by lyophilization. Lyophilized extracts were resuspended in 10 mL of 5% (v/v) acetic acid and applied to model 491 Prep Cell device (Bio-Rad) filled with acid native polyacrylamide gel consisting of stacking gel (10% T, 3% C) and separating gel (16% T, 3% C), then electrophoresed at 200 V. Eluents were fractionated from the anodal reservoir with 5% (v/v) acetic acid at a flow rate of 1 mL/min and 10 mL/fraction. To determine the fractions containing proteins, 1/20 volume of each fraction was electrophoresed on AU-polyacrylamide gel (12.5% T, 3% C) at 150 V[46], then proteins were visualized by staining with Coomassie Blue R-250.

AU-PAGE western blot

Samples (1/20 vol of fractions containing proteins extracted from the small intestinal tissue) were separated by AU-PAGE at 150 V and transferred to 0.1 μm nitrocellulose membrane (GE Healthcare) using a semidry apparatus (ADVANTEC) at 2.5 mA/cm^2 for 30 min. Chemically synthesized ox and rCrp1 prepared as described[47] were used as standards. The membranes were blocked by incubation with BSA-free StabilGuard immunoassay stabilizer (Surmodics) at room temperature for 1 h, reacted with biotinylated anti-Crp1 antibody (1 μg/mL, 76-R29, self-produced) which detects both ox and rCrp1–4 and 6 at 4^{o}C overnight. After washing, membranes were incubated with HRP-conjugated streptavidin (GE Healthcare) at room temperature for 1 h. After incubation, blots were visualized by Chemi-Lumi One Ultra.

Enteroid culture and Paneth cell live imaging

Enteroid culture and Paneth cell live imaging was conducted by previously described method[45,48]. Briefly, crypts were isolated from the proximal half of small intestines of 18–20 w ICR or SAMP1/YitFc mice and cultured in matrigel (Corning). After 3 days culture, enteroids were transferred onto collagen-coated glass bottom 8-well chamber cover slips (Matsunami) at 100 enteroids/well. To stimulate Paneth cell granule secretion, 10 mM carbachol (CCh, Sigma-Aldrich) was added to the culture medium. Differential interference contrast (DIC) images of Paneth cells in enteroids were acquired by confocal microscopy (A1, Nikon) before and 10 min after adding CCh

stimulation. For quantification of Paneth cell granule secretion, Paneth cell granule area were measured from DIC images of Paneth cells by using NIS-Elements AR, and percent area granule secretion were calculated as before[45]. To determine whether Paneth cell survive after granule secretion, enteroids were exposed to 10 μM CellEvent™ caspase-3/7 Green Detection Reagent (Thermo Fisher Scientific) in the culture medium and time-lapse images of Paneth cells stimulated by 10 μM CCh were obtained at 15 frames/sec at low laser power. Twenty-seven ICR mouse Paneth cells, and 24 SAMP1/YitFc mouse Paneth cells were analyzed.

Quantification of fecal cryptdin

From each mouse, fecal pellets were collected and dried by lyophilization. After lyophilization, fecal pellets were pulverized to powder using a bead beater-type homogenizer lT-12 (TAITEC). One hundred μL of 30% (v/v) acetic acid was added to 10 mg of fecal powder and vortexed at 4ºC overnight. After the vortex mixing, precipitates were removed by centrifugation (15,000 g for 30 min) at 4ºC. Supernatants were collected and concentrated by a Speed-Vac concentrator (Thermo Savant). Then, fecal precipitates were resuspended in 20 μL of PBS (-). Trypsin (Thermo Fischer Scientific) was dissolved in PBS (-) and adjusted to 20 ng/μL. One μL of suspension and 9 μL of trypsin solution were mixed and incubated at room temperature for 1 h. Tryptic digests of fecal samples were separated by Tris-Tricine SDS-PAGE[49] at 30 mA/gel and transferred to 0.22 μm PVDF membranes at 1.3 V for

7 min using Trans-Blot Turbo Transfer system. After the transfer, membranes were treated as described above. For quantification of Crps, band intensities were determined by ImageJ software.

DNA purification

Fresh fecal samples were collected from each mouse immediately after excretion. Collected feces were immediately snap-frozen and stored at -80ºC. Total genomic DNA was extracted and purified from 200 mg fecal samples using QIAamp Fast DNA Stool Mini Kit (QIAGEN) following the manufacturer's protocol. Final DNA concentrations were determined based on 260 nm absorbance using a Nanodrop 2000 spectrometer (Thermo Fischer Scientific).

16S rDNA sequencing

16S ribosomal RNA genes were amplified by PCR from each fecal DNA sample using universal primer set of Bakt 341F (5-cctacgggnggcwgcag) and Bakt 805R (5-gactachvgggtatctaatcc) which covers the V3-V4 variable region[50]. 1st PCR amplification was conducted in 25 μL-volume reaction mixtures containing 12.5 ng of fecal DNA, 200 nM of each primer and 1x KAPA HiFi Hot Start Ready Mix (Kapa Biosystems) under the following conditions: 95°C for 3 min, 25 cycles of 95°C for 30 sec, 55°C for 30 sec and 72°C for 30 sec, followed by 72°C for 5 min. 1st PCR products were purified with AMPure XP beads (Beckman Coulter). After purification, 2nd PCR was conducted for adding

sequencing adapters containing sample specific 8 bp barcodes to the 3'- and 5'- ends of 1st PCR products by using the Nextera XT Index Kit v2 Set B (Illumina). 2nd PCR amplification was conducted in 50-μL of reaction mixtures containing 5 μL of 1st PCR amplicon, 5 μL of each indexing primer and 1x KAPA HiFi Hot Start Ready Mix under the following conditions: 95°C for 3 min, 8 cycles of 95°C for 30 sec, 55°C for 30 sec and 72°C for 30 sec, followed by 72°C for 5 min. Each amplicon was purified, quantified using the Qubit dsDNA HS Assay Kit (Invitrogen), and then adjusted to 4 nM. 2nd PCR Amplicons were pooled 4 μL each and subjected to quantification using KAPA Library Quantification Kit Lightcycler 480 qPCR Mix (Kapa Biosystems) and then diluted to 4 pM. The amplicon library was combined with 5% equimolar PhiX Control v3 (Illumina), and sequenced on a MiSeq instrument using the MiSeq 600-cycle v3 kit (Illumina) by pair-end sequencing mode.

16S rDNA-based taxonomic analysis

Illumina pair-end reads FASTQ files were obtained by 16S rDNA sequence. After demultiplexing, OTU classification and diversity analyses were conducted by using QIIME version 1.9.1[51] according to previously described method (http://doi.org/10.5281/zenodo.1439555). Briefly, adapter sequences and low-quality bases were trimmed from both 5'- and 3' end of sequenced reads by BBDuk and pair-end reads were merged by BBmerge. Both BBDuk and BBmerge are included in the BBtools software suite (http://jgi.doe.gov/data-and-tools/bbtools/). After pair-end merge, chimeric sequences were

filtered by UCHIME[52]. Sequences with ≧ 97% similarity were binned as OTUs. The OTUs were classified taxonomically into five rank categories (phylum, order, class, family and genus) by using the SILVA 12_8 reference database by using UCLUST[53]. As α-diversity indexes, observed OTUs and PD whole tree were calculated. As β-diversity indexes, β-diversity unweighted UniFrac distance was calculated and visualized with Principal Coordinate Analysis. Statistical significance of β-diversity was determined by PERMANOVA in Qiime workflow.

Antibiotic treatment

SAMP1/YitFc mice were subjected to antibiotic (Abx) treatments for 6 weeks from 4 to 10 w as described[54]. Briefly, 1 g/L ampicillin sodium salt (Sigma-Aldrich) dissolved in drinking water and administered *ad libitum*. Ampicillin supplemented drinking water was renewed every 7 day. In addition, 10 mL/kg body weight of an antibiotic cocktail consisting of 5 mg/mL vancomycin hydrochloride (Wako pure chemical industries), 5 mg/mL neomycin trisulfate salt hydrate (Sigma-Aldrich), and 10 mg/mL metronidazole (Sigma-Aldrich) dissolved in distilled water were prepared at time of use and orally administered every 12 h via silicon sonde (Fuchigami kikai) to Abx-treated mice. As a control, distilled water containing no antibiotics was administered *ad libitum* and orally administered via silicon sonde to water-treated mouse. Fresh fecal samples from each mouse were collected at before and after the experiments. Total DNA was purified from fecal samples and

subjected to PCR amplification as described in 16S rDNA sequencing. To test whether the intestinal microbiota was removed, PCR products from each fecal sample were electrophoresed in agarose gels and visualized by ethidium bromide staining.

Bactericidal assays

Anaerotruncus coliholminis JCM 15631 was obtained from the Institute of Physical and Chemical Research (RIKEN). The bacterium was cultured in Eggerth-Gagnon (EG) liquid medium supplemented with defibrinated horse blood under anaerobic conditions using the Anaero Pack system (Mitsubishi Gas Chemical) at 37°C. Exponential-phase bacterial culture was centrifuged 3,000 g for 5 min at 4°C, washed twice, and then resuspended in PBS (-) diluted 1:1 with Milli-Q water. Bacterial cell number was determined by OD_{600}. Fifty μL of suspension containing 1,000 colony-forming units (CFU) per aliquot were mixed with equal volumes of ox or rCrp1 to final concentrations from 0 to 1.35 μM, incubated under anaerobic conditions at 37°C for 1 h, and mixtures were plated on EG agar plates and incubated anaerobically at 37°C until visible colonies appeared. Bacterial survival rates at each concentration were calculated from the number of surviving colonies relative to peptide-unexposed controls.

Rectal administration of reduced-form Crp1

For habituation against the stimuli by rectal administration, 5 w ICR mice were rectally administrated 200 μL of distilled water once in two day for 7 days. After the acclimation period, fresh fecal samples for microbiota analyses were collected at day 0, day 2 and day 4. At day 1 and day 3, single doses of 200 μL of 1 mg/mL rCrp1 dissolved in distilled water or 200 μL of distilled water were administered rectally to rCrp1-treated mice or control mice, respectively. Substances were carefully deposited to a depth of 2 cm by using stainless steel sonde.

Statistical analyses

All statistical analyses were conducted by using the Prism ver. 7.0 software (GraphPad). Two-sided tests were performed in all experiments. Between 2 groups, statistical significance was determined by Student's T test or Mann-Whitney's U test. One-way ANOVA followed by Tukey's post hoc test was used for more than three groups, and two-way ANOVA followed by Bonferroni post hoc test was used for repeated measurements. Correlation analysis was performed by Pearson's correlation coefficients test. $p < 0.05$ was considered statistically significant.

Data availability

Raw sequencing files for the 16S rDNA sequencing data sets are deposited at Sequence Read Archive (PRJNA622264, PRJNA622384).

3. Results

3.1 Relationships between ER stress in Paneth cells and ileitis progression of SAMP1/YitFc, a murine model of Crohn's disease

3.1.1 Number of abnormal Paneth cells increases along with disease progression of SAMP1/YitFc mice

First, histological analysis with Hematoxylin-Eosin staining was conducted to assess the relationship between disease progression and Paneth cells in SAMP1/YitFc mice, which develop spontaneous ileitis by 20 weeks of age (w) which resembles that of CD patients[41]. In SAMP1/YitFc mice, progression of ileitis was observed from 4 to 20 w characterized by inflammatory cell infiltration, crypt elongation, thickening of muscle layer, and crypt abscess (Fig 1A-F). Inflammatory scores were significantly elevated from 10 to 20 w (Table 1 and Fig 1G; 4 w: 0.19 ± 0.08, 10 w: 1.00 ± 0.22, 20 w: 2.74 ± 0.49). At 10 and 20 w, abnormal Paneth cells were observed not only at the base of crypts but also in the upper part of crypts and on villi, where Paneth cells are absent in controls (Fig. 1A). Also, the number of abnormal Paneth cells increased significantly from 4 to 10 w (Fig 1C, 4 w: 3.54 ± 0.16; 10 w: 6.34 ± 0.63; 20 w: 8.30 ± 0.90 cells/crypt-villus axis). Moreover, eosinophilic granule-positive cells at 10 and 20 w also stained positive for alcian blue which detects mucus normally

produced by goblet cells (Fig 2B) and co-expression of Crps and Muc2, indicating that the abnormal Paneth cells may be intermediate cells which have properties common to both Paneth and goblet cells[55]. To address possible mechanisms of abnormal Paneth cell accumulation in the upper crypts and villi, expression of EphrinB2, which is known to regulate the position of Paneth cells at the base of the crypt[56] by immunofluorescent staining. Along with disease progression, the EphB2 expression was decreased in crypts of abnormal Paneth cells, and no EphB2 expression was observed in abnormal Paneth cells on villi or in the crypts at 20 w (Fig 2D), suggesting that the decreased expression of EphB2 accompanying disease progression allows for the transfer of Paneth cells onto the villi. Furthermore, a strong positive correlation was shown between the number of abnormal Paneth cells and the inflammatory scores of individual SAMP1/YitFc mice (Fig 2E). These data indicated that the increase of abnormal Paneth cells is associated with disease progression in SAMP1/YitFc mice.

3.1.2 Abnormal Paneth cells exhibit ER stress

To observe abnormal SAMP1/YitFc mouse Paneth cells at higher resolution, transmission electron microscopy (TEM) was performed. Paneth cells in control mice had electron dense granules of uniform size in the apical region (Fig 3A). In contrast, abnormal Paneth cells of SAMP1/YitFc mice contained granules of non-uniform-size with electron-lucent halos in the granule periphery (Fig 3B). These abnormalities in Paneth cell granule morphology were more evident and prominent in 20 w

SAMP1/YitFc mice than in 4 w animals. In addition, the ER structure of control mouse Paneth cells displayed orderly, stacked ER cisternae around nuclei, but SAMP1/YitFc mouse Paneth cells showed swollen, disordered ER structures, which are characteristic of ER stress, from 4 w to 20 w. These ER abnormalities were observed in all Paneth cells randomly selected from three 20 w SAMP1/YitFc mice (Fig 3C, D). Paneth cell abnormalities were quantified using TEM images (Fig 3E). In SAMP1/YitFc mice, the number of granules increased significantly at 20 w compared to 4 w (Fig 3F; 4 w: 19.0 ± 2.2 and 20 w: 28.1 ± 2.0 granules/Paneth cell). In addition, ER luminal diameter increased significantly at 20 w compared to 4 w (Fig 3G; 4 w: 0.054 ± 0.005 and 20 w: 0.097 ± 0.002 μm), which indicates accumulation of ER stress in abnormal Paneth cells from cellular morphology. To prove the ER stress in abnormal Paneth cells at molecular levels, expression of UPR-related molecules, which reflect ER stress intensity, in isolated ileal crypts were analyzed (Fig 4A, B). In SAMP1/YitFc mice, although pIRE1α expression was not statistically (20 w ICR mice: 0.45 ± 0.07, 4 w and 20 w SAMP1/YitFc mice: 0.65 ± 0.11 and 0.82 ± 0.13), ATF4 (0.69 ± 0.07, 0.48 ± 0.03 and 1.20 ± 0.24), cleaved-ATF6 (0.69 ± 0.07, 0.48 ± 0.03 and 1.20 ± 0.24) and GRP78 (0.44 ± 0.07, 0.18 ± 0.06 and 0.85 ± 0.29) in ileal crypts was significantly increased in SAMP1/YitFc mice at 20 w compared to those at 4 w along with disease progression (Fig 2F). To clarify whether ER stress in the crypts determined by western blot occurs in Paneth cells, immunofluorescent staining of the expression of ER stress markers; GRP78 and calreticulin in ileal tissues of both ICR and SAMP1/YitFc mice were performed. In SAMP1/YitFc

mice at 20 w, the expression of both GRP78 and calreticulin was remarkably increased in abnormal Paneth cells, in contrast to low expression in ICR mice (Fig 5A, B). Furthermore, expression level of transcription factor, MIST1, which is known to suppress ER stress and is specifically expressed in Paneth cells of the intestinal epithelium[57] was analyzed. MIST1 was strongly expressed in the nucleus of Paneth cells in 20 w ICR mice. In sharp contrast, MIST1 expression was dramatically diminished at 20 w compared to 4 w in SAMP1/YitFc mouse Paneth cells (Fig 5C). These results indicated that ER stress occurs in abnormal Paneth cells of SAMP1/YitFc mice.

3.2 Relationships between secretion of reduced-form α-defensin into the intestinal lumen and disease progression

3.2.1 Abnormal Paneth cells synthesize reduced-form α-defensin

Because abnormal Paneth cells exhibited ER stress, we next examined whether rCrps are produced in these cells due to misfolding of disulfide bonds. Crps consist of multiple isoforms with extensive similarities in amino acid sequences[58]. We purified Crps from small intestinal tissues and analyzed their tertiary structures by acid urea (AU)-PAGE western blot using a pan-Crp antibody

which detects both ox and rCrp isoforms (Fig 6A). In AU-PAGE, oxCrp1 showed the lowest mobility among oxCrps, and oxCrp1 showed higher mobility than all rCrps (Fig 6B). Thus, using oxidized and reduced-forms of chemically synthesized Crp1[47] as markers for evaluating tertiary structure, Crps in small intestinal tissue detected with lower mobilities than oxCrp1 were judged to be rCrps, while peptides with higher mobilities were judged to be oxCrps. rCrps were detected in 20 w SAMP1/YitFc mice but were not found in age-matched controls or in 4 w SAMP1/YitFc mice (fractions 3-10 in Fig 7). Multiple bands of rCrps with different mobilities were detected in these fractions, suggesting that numerous isoforms were misfolded. In addition, levels of oxCrps increased in 20 w (fraction 1 and 2 in Fig 7) compared to 4 w SAMP1/YitFc mice and controls. These results indicate that abnormal Paneth cells produce rCrps, which are not detected in the normal state, coincident with progression of ER stress.

3.2.2 Abnormal Paneth cells secrete reduced-form α-defensin along with disease progression

To clarify whether the rCrps that accumulate in abnormal Paneth cells are secreted into the intestinal lumen, we quantified rCrps in mouse feces. Because electrophoresis of fecal extracts was inhibited perhaps by fecal contaminants, distinguishment of ox and rCrps in feces by AU-PAGE western blots was not feasible. Therefore, establishment of the novel system for distinguishing and

quantifying ox and rCrps in feces was conducted. oxCrps are known to resist degradation by digestive enzymes *in vitro*, in contrast to Crp mutants that lack one or more disulfide bonds and are easily degraded[59]. Using this property of Crps, mouse fecal extracts were treated with trypsin, then Crps in feces were separated and quantified by western blotting after denatured tricine SDS-PAGE separations. We then quantified ox and rCrps by comparing the quantity of Crps in trypsin-treated and untreated samples (Fig 8). Trypsin treatment of a synthetic, rCrp1 peptide standard caused gel bands to disappear completely, in contrast to oxCrp1 bands, which were unaffected by trypsin exposure. Therefore, we implemented this method for measuring ox and rCrps based on the sensitivity to trypsin. In control and 4 w of SAMP1/YitFc mice, band intensities of Crps detected in fecal extracts showed no significant changes resulting from trypsin digestion. However, Crps levels in fecal extracts from 20 w of SAMP1/YitFc mice were significantly decreased by trypsin digestion (Fig 8A and B), showing that rCrps produced by abnormal Paneth cells were secreted into the intestinal lumen and sensitive to proteolysis. Accordingly, we quantified ox and rCrps in feces on the basis of their sensitivity to trypsin. For example, Crps detected in fecal samples not subjected to tryptic digestion was considered to be total Crps, i.e., the sum of ox and rCrps, and Crps detected in fecal samples treated with trypsin was identified as oxCrps. Therefore, values obtained by subtracting the quantity of Crps after trypsin treatment from that of samples not treated with trypsin were taken to be the amount of rCrps (Fig 9C). Levels of oxCrps in feces of SAMP1/YitFc mice approximately doubled at 20 w compared to 4 w (4

w: 6.50 ± 1.46 and 20 w: 11.76 ± 1.51 ng/500 μg feces). In sharp contrast, the quantity of rCrps in feces of 20 w SAMP1/YitFc mice increased approximately 40-fold compared to 4 w animals (4 w: 0.23 ± 0.49; 20 w: 9.82 ± 3.12 ng/500 μg feces). Therefore, rCrps, which were almost undetectable before disease onset, are secreted into the intestinal lumen at high levels during disease progression. In control feces, the amount of oxCrps secreted was unchanged during the first 20 weeks, and rCrps was not detected (Fig 8C). To test whether synthesis of rCrps is involved in IBD progression, correlation analyses between the quantity of ox and rCrps levels in feces and the inflammatory scores of individual SAMP1/YitFc mice were conducted (Fig 8D). A strong positive correlation existed between the levels of rCrps and inflammatory scores, but no significant correlation was observed between quantities of oxCrps and inflammatory scores. Therefore, it was indicated that rCrps accumulated in the intestinal lumen was associated with the disease progression in SAMP1/YitFc mice.

To clarify whether rCrps detected in feces of SAMP1/YitFc mice were secreted from abnormal Paneth cells, Paneth cell granule secretion was visualized and quantified using enteroids, three-dimensional *ex vivo* cultures of small intestinal epithelial cells, including Paneth cells[45]. Using carbachol (CCh) to induce granule secretion of Paneth cells in enteroids, granule secretion ratio of the SAMP1/YitFc-mouse derived Paneth cells was equivalent to that of ICR mouse Paneth cells (Fig 9A; 56.55 ± 2.85 vs 46.97 ± 4.44%). In addition, we tested whether abnormal Paneth cells survived during and after secretion, i.e., did not undergo cell death. After treatment of SAMP1/YitFc mouse enteroids

with a fluorescent probe specific to active caspase-3/7 as reported previously[18], granule secretion was induced by CCh. No cleaved caspase was detected in Paneth cells during or after secretion (Fig 9B). These results showed that abnormal Paneth cells in SAMP1/YitFc mice are able to secrete granules and released rCrps along with disease progression by granule secretion.

3.3. Relationships between secretion of reduced-form α-defensin and dysbiosis along with disease progression

3.3.1 Dysbiosis occurs along with disease progression of SAMP1/YitFc mice

Because rCrps has been known to elicit an abnormal bactericidal spectrum *in vitro* against commensal bacteria compared to oxCrps[39], we tested whether rCrps secreted into the intestinal lumen induce dysbiosis in SAMP1/YitFc mice. Firstly, we determined whether dysbiosis occurs in SAMP1/YitFc mice using 16S rDNA metagenomic sequencing of the intestinal microbiota in fecal samples. In β-diversity analysis, there was no significant difference between control and SAMP1/YitFc mice, whereas the intestinal microbiota of SAMP1/YitFc mice showed significantly different composition compared to control mice at 20 w, indicating that SAMP1/YitFc mice shaped

different microbiota composition to control mice along with the disease progression (Fig 10).

To analyze shifts of the microbiota composition along with the disease progression, comparison of 4 w and 20 w SAMP1/YitFc mice was conducted. Both two α-diversity indexes, phylogenic diversity (PD) whole tree (Fig 11A; 4 w: 15.61 ± 0.56 and 20 w13.64 ± 0.44) and operational taxonomic units (OTUs) (Fig 11B; 4w: 194.88 ± 7.40 and 20 w: 158.68 ± 7.01) were decreased significantly during disease progression. In addition, significant decreases of Lachnospiraceae (34.37 ± 1.89 and 24.86 ± 1.65%) and Ruminococcaceae (9.70 ± 0.83 and 6.83 ± 1.00%) and increases of Bacteroidaceae (29.82 ± 1.75 and 35.67 ± 1.71%) and Rikenellaceae (5.64 ± 0.96 and 8.69 ± 1.05%) were observed at the family level in 20 w compared to 4 w mice (Fig 11C). At the genus level, a significant decrease of *Lachnospiraceae;Other* (6.23 ± 1.08 and 3.36 ± 0.66%) and *Anaerotruncus* (0.74 ± 0.17 and 0.38 ± 0.07%) and an increase of *Bacteroides* (29.82 ± 1.75 and 35.67 ± 1.71%) was shown in 20 w (Fig 11D). To clarify further whether the dysbiosis that occurred in 20 w SAMP1/YitFc mice relates to disease progression, correlation analyses between the microbiota composition and individual inflammatory scores were performed. Negative correlations were observed between each α-diversity index and inflammatory scores (Fig 11E and F). Moreover, at the genus level, relative abundance of *Lachnospiraceae;Other* and *Anaerotruncus* correlated negatively and *Bacteroides* correlated positively with the inflammatory score (Fig 11G). In contrast, there were no significant changes in both α-diversity and relative abundance of these genera in control mice along

with age in weeks (Fig 12). Thus, dysbiosis with decreased diversity and compositional changes in certain taxa accompanies disease progression in SAMP1/YitFc mice.

3.3.2 Secretion of reduced-form α-defensin positively correlates with dysbiosis

To clarify the relationship between secretion of rCrps into the intestinal lumen and dysbiosis occurred along with the disease progression of SAMP1/YitFc mice, correlation analysis between the quantity of rCrps in feces and α-diversity indexes of individual animals was conducted. A strong negative correlation was observed between the two α-diversity indexes decreased along with the disease progression and the amount of rCrps (Fig 13A and B). Furthermore, strong negative correlations were found between levels of rCrps and the occupancy of *Lachnospiraceae;Other* and *Anaerotruncus*, but there was a strong positive correlation with *Bacteroides* (Fig 13C). In contrast, no correlation was observed between the amount of oxCrps in feces, the diversity indexes, or bacterial composition of the fecal microbiota (Fig 14). *In vitro,* rCrp1 had significantly stronger bactericidal activity than oxCrp1 against *Anaerotruncus coliholminis*, a commensal bacterium of the genus *Anaerotruncus* that induces regulatory T cell differentiation in the intestine[4], suggesting that rCrps show different bactericidal spectrums against the commensal bacteria which significantly shifted along with the disease progression of SAMP1/YitFc mice (Fig 15). These results indicated that rCrps

secreted into the intestinal lumen is associated with dysbiosis observed in SAMP1/YitFc mice along with the disease progression.

3.4. Causal relationships between secretion of reduced-form α-defensin and dysbiosis

3.4.1. Reduced-form α-defensin is secreted into the intestinal lumen independently of the intestinal microbiota existence

Next, causal relationships between secretion of rCrps and dysbiosis were analyzed. To exclude that dysbiosis could lead to Paneth cell defects, Paneth cell morphology and rCrps secretion of SAMP1/YitFc mice were analyzed after depletion of the intestinal microbiota by antibiotics (Abx) treatment from 4 w to 10 w (Fig 16A). The PCR of fecal 16S rDNA confirmed that intestinal bacteria could be eliminated completely by oral administration of Abx (Fig 16B). The number of eosinophilic granule positive cells, i.e., abnormal Paneth cells, per villus-crypt axis in Abx-treated group was similar to water-treated mouse at 10 w in SAMP1/YitFc mice (Fig 16C; water-treated: 5.20 and Abx-treated: 4.25 ± 0.70 cells/crypt-villus axis). In addition, TEM analyses showed ER swelling in Paneth cells of Abx group, as in water-treated mice (Fig 16D; water-treated: 0.078 and Abx-treated: 0.070 ± 0.001 μm). Furthermore, it was confirmed that rCrps were present in feces of both the Abx group and water-treated mice (Fig 16E; water-treated: 8.06 and Abx-treated: 6.35 ± 1.33 ng). These data that

Paneth cells in SAMP1/YitFc mice retained morphological abnormalities and rCrps secretion to the intestinal lumen even after Abx treatment, strongly suggests that appearance of abnormal Paneth cells and secretion of rCrps precede dysbiosis along with disease progression of SAMP1/YitFc mice.

3.4.2 Reduced-form α-defensin secreted into the intestinal lumen alters the intestinal microbiota

Finally, we further tested whether reduced-form Crps could change the intestinal microbiota using ICR mice (Fig 17A). Because rCrp4 have been reported to be degraded by proteases *in vitro*[40,59] and considering that oral administration of rCrps may result in degradation in the stomach and loss of activity in the intestinal lumen, we administered rCrp1 rectally. Although short-term rectal administration of rCrp1 (4 days) to ICR mice did not replicate the SAMP1/YitFc mouse enteropathy, observed OTUs indicating α-diversity in the rCrp1 group were significantly decreased compared to the control group at day 4 (Fig 17B; water-treated and rCrp1-treated group: 274.00 ± 4.16 and 277.25 ± 8.64 at day 0, 292.67 ± 7.86 and 249.25 ± 22.48 at day 2, 305.33 ± 3.18 and 241.00 ± 20.06 at day 4). Furthermore, Lachnospiraceae (14.59 ± 2.83 vs 13.96 ± 0.48% at day 0; 18.97 ± 4.14 vs 10.61 ± 0.46% at day 2; 24.90 ± 6.48 vs 13.13 ± 1.21% at day 4) and Ruminococaceae (6.28 ± 0.24 vs 6.34 ± 0.70% at day 0; 7.22 ± 0.85 vs 3.05 ± 0.62% at day 2; 8.51 ± 1.28 vs 3.76 ± 0.89% at day 4) both which were decreased along with disease progression of SAMP1/YitFc mice (Fig 11C), were also significantly decreased in the rCrp1 group, at day 4 and at day 2 and day 4, respectively (Fig 17C),

showing that rCrp1 modulated the intestinal microbiota composition *in vivo*. Taken together, our results showed that rCrps which were synthesized and secreted into the intestinal lumen from ER-stressed abnormal Paneth cells could be involve dysbiosis associated with disease progression in SAMP1/YitFc mouse model of CD.

4. Discussion

4.1 Dysbiosis and functional deficiencies of α-defensin in pathogenesis of Crohn's disease

Reduced diversity of the intestinal microbiota, dysbiosis, observed in SAMP1/YitFc mice is consistent with previous studies of the intestinal microbiota of CD patients from the America, Europe, and Japan[34,60–62]. Furthermore, decreases of both Lachnospiraceae and Ruminococaceae along with disease progression shown here also have been reported in CD patients in the America and Japan[34,62,63], and the increase of Bacteroidaceae which is observed in SAMP1/YitFc mice is also consistent with previous studies about CD patients in UK and Canada[60,64]. Therefore, dysbiosis in SAMP1/YitFc mice shown in this study have some common features with those of CD patients. Because SAMP1/YitFc mice spontaneously develop ileitis which shows many common features to CD patients[41] and show the improvement of the disease state by clinical treatments for CD such as administration of TNFα antibody[65] and steroid anti-inflammatory drugs[66], this model is considered to be a suitable model for analyzing the pathogenesis and pathophysiology of CD[43]. This study suggests further that this mouse model is suitable for analyzing the effects of dysbiosis on pathophysiology of CD.

Failures in homeostasis of both the immune system and epithelial cells in the intestine via dysbiosis has been considered to contribute to the pathophysiology of CD[20]. Because Lachnospiraceae

and Ruminococcaceae produce butyrate[67], an inducer of regulatory T cell differentiation[2], decreases of these bacteria shown in this study may lead to excessive adaptive immune responses in the intestine. Moreover, Bacteroidaceae, which increased in SAMP1/YitFc mice along with disease progression, includes some opportunistic pathogens[68], thus their overgrowth may induce enteric mucosal inflammation. Certain Rikenellaceae which also increased in SAMP1/YitFc mice produce capnine, a sulpholipid inhibitor of the vitamin D receptor[69,70]. Because activation of the vitamin D receptor upregulates transcription factors for antimicrobial peptides including LL-37[71] and α-defensin[72] and genetic deletion of the vitamin D receptor in intestinal epithelial cells leads to reduction of autophagy[73], increased Rikenellaceae may disrupt innate enteric immunity and result in epithelial cell dysfunction. These findings indicate that dysbiosis observed in SAMP1/YitFc mice associates with the pathophysiology of ileitis via induction of excessive immune responses and injury of epithelial cells in the intestine.

Recently, importance of Paneth cells, one of the major small intestinal epithelial lineages, and α-defensin, an antimicrobial peptide secreted by Paneth cells, have been recognized[14]. It is also reported that abnormal localization of secretory granules containing α-defensin in Paneth cells of CD patients has been reported in association with progression of dysbiosis and an increase of relapse rates[34,74], suggesting that functional deficiencies of Paneth cells and α-defensin relate to dysbiosis in the pathogenesis of CD. However, expression levels of HD5, a human Paneth cell α-defensin, have

been reported to decrease in ileum[75] or contrary elevate in colon due to appearance of ectopic Paneth cells[76] of CD patients, so that the relationship between CD and the amount of HD5 remain controversial. This study reveals that rCrps is produced in Paneth cells of SAMP1/YitFc mice due to misfolding of disulfide bonds and further secreted into the intestinal lumen, and associate with the disease progression via dysbiosis. These results introduce a novel mechanism of CD pathogenesis that not just quantitative but qualitative disorders of α-defensin induce pathology of the disease via dysbiosis for the first time.

4.2. Relationships between ER stress in Paneth cells and Crohn's disease

Previously, relationships between CD pathogenesis and ER stress in Paneth cells have been reported. Genes involved in resolving ER stress, e.g., UPR-related *XBP1*[29] and *AGR2*[30], autophagy-related *ATG16L1*[31], *IRGM1*[32], and *LRRK2*[33] are known as susceptibility genes for CD, and deletions or mutations in these genes to lead to Paneth cell abnormalities. In addition, environmental risk factors of CD such as high-fat diet[25] and zinc deficiency[77] induce ER stress in Paneth cells[78,79], and vitamin D deficiency, which is also a CD risk factor, induces defective autophagy in mouse Paneth cells[73]. suggesting that diverse environmental factors may induce ER stress in Paneth cells. These studies imply that both genetic and environmental factors of CD induce ER stress in Paneth cells. Moreover,

CD patients that have ER stressed-Paneth cell due to *ATG16L1* gene mutations are colonized by enteroinvasive-*Escherichia coli* which induce enteritis in higher rates[35]. Thus, the relationship between ER stress in Paneth cells and dysbiosis in CD has been suggested, although the mechanisms that link ER stress and dysbiosis remain unclear. To clarify these mechanisms, relationships between ER stress in Paneth cells and disease progression of SAMP1/YitFc mice were analyzed in this study.

This study showed that aberrant cellular localization of abnormal Paneth cells increases along with disease progression, consistent with previous reports that intermediate cells with immature granules appear and increase in crypts and on lower regions of villi in SAMP1/YitFc mice[55]. Furthermore, excessive ER stress in the abnormal Paneth cells was revealed by analyses of the cellular morphologies and the molecular expression patterns. Expression level of MIST1, an inhibitor of ER stress regulated in downstream of XBP1[80] was decreased in abnormal Paneth cells, suggesting that SAMP1/YitFc mice partially share the pathways of ER stress induction with CD patients. It is reported that MIST1 regulates cell polarity, size, and intracellular junction integrity of pancreatic acinar cells belonging to the secretory epithelial cell lineage same as Paneth cells[81]. It is also reported that intermediate cells showing similarities to abnormal Paneth cells in SAMP1/YitFc mice appear in the small intestine of *MIST1* knockout mice[57]. These reports suggest that insufficient activation of MIST1 against ER stress may be one factor of appearance of abnormal Paneth cells in SAMP1/YitFc mice.

ER stress induces misfolding of disulfide bonds during protein synthesis in cells[37]. α-

Defensin is rich in Cys residues and characterized by three intramolecular disulfide bonds in their tertiary structures[82,83]. Because excessive ER stress accumulated in abnormal Paneth cells of SAMP1/YitFc mice, it was hypothesized that rCrps with no disulfide bonds are synthesized in these cells and further secreted into the intestinal lumen. This study revealed that abnormal Paneth cells produced rCrps and secreted it along with the disease progression of SAMP1/YitFc mice. These findings indicate for the first time that excessive ER stress in Paneth cells may cause misfolding of α-defensin, regulators of the intestinal microbiota and provide new insights in understanding the relationships between ER stress in Paneth cells and other diseases.

4.3. Mechanisms of the intestinal microbiota regulation based on structure-function relationships in α-defesnin

Previously, it was reported that oxCrps elicit no or minimal bactericidal activity against 8 species of commensal bacteria including *Bifidobacterium bifidum* and *Lactobacillus casei* whereas rCrps kill these commensals[39], indicating that selective bactericidal activities of α-defensin are regulated by the formation of intramolecular disulfide bonds. Therefore, this study analyzed the relationship between dysbiosis and secretion of rCrps into the intestinal lumen of SAMP1/YitFc mice. In this study, rCrps were only detected in SAMP1/YitFc mice after the disease onset showing dysbiosis. Furthermore, rCrps in feces positively correlated with dysbiosis, whereas no significant correlation

was not shown between oxCrps. In *in vitro* bactericidal assays, rCrp1 elicited significantly greater potency than oxCrp1 against *Anaerotruncus coliholminis*, which decreases in SAMP1/YitFc mice along with the disease progression. Moreover, rectal administration of rCrp1 to normal ICR mice partially reproduced the common features to the intestinal microbiota in SAMP1/YitFc mice after disease progression such as decrease of α-diversity and occupancy of Lachnospiraceae and Ruminococcaceae. These results suggest that rCrps induce dysbiosis by exhibiting different bactericidal spectrums against commensals compared to oxCrps, showing new mechanism of the intestinal microbiota regulation by α-defensin in its tertiary structure-dependent manners.

Although the factors that determine the differential bactericidal spectra of ox and rCrps remain unclear, selective permeabilization of bacterial cell membranes by ox and rCrps is a possibility. In part, this notion is supported findings that Crp4 variants that do not form disulfide bonds accumulate at bacterial membrane surfaces, while oxCrp4 binds to bacterial membranes and translocates into them[84]. Also, rCrp4 may cause stronger membrane depolarization than oxCrp4 peptides[39]. In this study, we have also shown that rCrps secreted into the small intestinal lumen by Paneth cells reach the colonic lumen and can be recovered in feces. Reduced-form α-defensin is sensitive to degradation *in vitro* by proteinases which also are abundant in the intestinal lumen[40,59]. Nevertheless, we recovered intact rCrps from feces, suggesting that mechanisms exist for protection from luminal proteinases. Perhaps, as has been reported for reduced-form HD5, proteolytic stability may result by forming complexes

with Zn^{2+} *in vitro*[85]. Also, fecal concentrations of the serine protease inhibitor α_1-antitrypsin increase in CD patients compared to healthy subjects[86]. Perhaps these and additional mechanisms protect reduced-form α-defensin from degradation in the intestinal lumen. We speculate that in CD patients such factors allow reduced-form α-defensin to persist and induce dysbiosis.

4.4 Future perspectives of this study in application to treatments in clinical practice

Differences in α-defensin bactericidal activities due to the presence or absence of disulfide bonds have been reported not only in mouse but also human. For example, reduced-form HD5 has lower bactericidal activities against *Escherichia coli* and *Staphylococcus aureus* compared to oxidized-form HD5[87]. Reduced-form HD6 inhibits the growth of certain commensal bacteria including *Bifidobacterium adolescentis*, whereas oxidized-form HD6 has no such effect[88]. Moreover, reduced-form HD5 has been detected in human ileal tissue[40] and also in the intestinal lumen[89]. These studies support the view that dysbiosis due to α-defensin misfolding may occur not only in a mouse model of CD but also in patients. Furthermore, ER stress in Paneth cells may be caused by varied environmental factors in addition to genetic risk factors, and Paneth cell defects accompanied by ER stress are associated with diseases related with dysbiosis such as obesity[90], ischemia/reperfusion[91], and alcoholic liver disease[92]. Possibly, α-defensin misfolding and the secretion of reduced-form α-defensin caused by ER stress in Paneth cells may also be associated with onset and progression of diseases. In the

future, comprehensive analyses including tertiary structure of α-defensin in the intestinal lumen, composition of the intestinal microbiota, and pathophysiology of dysbiosis-related diseases may identify new pathogenetic mechanisms triggered by α-defensin misfolding. Such findings should contribute further to the development of novel diagnostic methods and therapeutics that target reduced-form α-defensin.

5. Conclusion

This study shows that α-defensin misfolding caused by accumulation of ER stress in Paneth cells could induce the CD pathogenesis via dysbiosis by using SAMP1/YitFc, a murine model of CD. This study makes a substantial contribution to the development of novel diagnostics and therapeutics of CD targeting Paneth cells and reduced-form α-defensin by further clinical investigation.

6. References

1. Sender, R., Fuchs, S. & Milo, R. Are We Really Vastly Outnumbered? Revisiting the Ratio of Bacterial to Host Cells in Humans. *Cell* **164**, 337–340 (2016).

2. Nishijima, S. *et al.* The gut microbiome of healthy Japanese and its microbial and functional uniqueness. *DNA Research* **23**, 125–133 (2016).

3. Bäckhed, F. *et al.* The gut microbiota as an environmental factor that regulates fat storage. *Proceedings of the National Academy of Sciences* **101**, 15718–15723 (2004).

4. Atarashi, K. *et al.* Treg induction by a rationally selected mixture of Clostridia strains from the human microbiota. *Nature* **500**, 232–236 (2013).

5. Ma, Q. *et al.* Impact of microbiota on central nervous system and neurological diseases: the gut-brain axis. *Journal of Neuroinflammation* **16**, 53 (2019).

6. Kho, Z. Y. & Lal, S. K. The Human Gut Microbiome - A Potential Controller of Wellness and Disease. *Frontiers in Microbiology* **9**, 1835 (2018).

7. Selsted, M. E. & Ouellette, A. J. Mammalian defensins in the antimicrobial immune response. *Nature Immunology* **6**, 551–557 (2005).

8. Ouellette, A. J. *et al.* Developmental regulation of cryptdin, a corticostatin/defensin precursor mRNA in mouse small intestinal crypt epithelium. *The Journal of Cell Biology* **108**, 1687–1695 (1989).

9. Jones, D. E. & Bevins, C. L. Defensin-6 mRNA in human Paneth cells: implications for antimicrobial peptides in host defense of the human bowel. *FEBS Letters* **315**, 187–192 (1993).

10. Porter, E. M., Liu, L., Oren, A., Anton, P. A. & Ganz, T. Localization of human intestinal defensin 5 in Paneth cell granules. *Infection and Immunity* **65**, 2389–2395 (1997).

11. Wilson, C. L. *et al.* Regulation of intestinal alpha-defensin activation by the metalloproteinase matrilysin in innate host defense. *Science* **286**, 113–117 (1999).

12. Ayabe, T. *et al.* Secretion of microbicidal α-defensins by intestinal Paneth cells in response to bacteria. *Nature Immunology* **1**, 113–118 (2000).

13. Salzman, N. H., Ghosh, D., Huttner, K. M., Paterson, Y. & Bevins, C. L. Protection against enteric salmonellosis in transgenic mice expressing a human intestinal defensin. *Nature* **422**, 522–526 (2003).

14. Salzman, N. H. *et al.* Enteric defensins are essential regulators of intestinal microbial ecology. *Nature Immunology* **11**, 76–83 (2010).

15. Hayase, E. *et al.* R-Spondin1 expands Paneth cells and prevents dysbiosis induced by graft-versus-host disease. *The Journal of Experimental Medicine* **214**, 3507–3518 (2017).

16. Eriguchi, Y. *et al.* Graft-versus-host disease disrupts intestinal microbial ecology by inhibiting Paneth cell production of α-defensins. *Blood* **120**, 223–231 (2012).

17. Nakamura, K., Sakuragi, N., Takakuwa, A. & Ayabe, T. Paneth cell α-defensins and enteric microbiota in health and disease. *Bioscience of Microbiota, Food and Health* **35**, 57–67 (2016).

18. Eriguchi, Y. *et al.* Essential role of IFN-γ in T cell-associated intestinal inflammation. *JCI Insight* **3**, e121886 (2018).

19. Zuo, T. & Ng, S. C. The Gut Microbiota in the Pathogenesis and Therapeutics of Inflammatory Bowel Disease. *Frontiers in Microbiology* **9**, 2247 (2018).

20. Torres, J., Mehandru, S., Colombel, J.-F. & Peyrin-Biroulet, L. Crohn's disease. *Lancet* **389**, 1741–1755 (2017).

21. Burisch, J., Jess, T., Martinato, M., Lakatos, P. L. & ECCO-EpiCom. The burden of inflammatory bowel disease in Europe. *Journal of Crohn's and Colitis* **7**, 322–337 (2013).

22. Brusaferro, A. *et al.* Gut dysbiosis and paediatric Crohn's disease. *The Journal of Infection* **78**, 1–7 (2019).

23. Jostins, L. *et al.* Host-microbe interactions have shaped the genetic architecture of inflammatory bowel disease. *Nature* **491**, 119–124 (2012).

24. Shaw, S. Y., Blanchard, J. F. & Bernstein, C. N. Association Between the Use of Antibiotics and New Diagnoses of Crohn's Disease and Ulcerative Colitis. *American Journal of Gastroenterology* **106**, 2133–2142 (2011).

25. Hou, J. K., Abraham, B. & El-Serag, H. Dietary Intake and Risk of Developing Inflammatory Bowel Disease: A Systematic Review of the Literature. *The American Journal of Gastroenterology* **106**, 563–573 (2011).

26. Somineni, H. K. & Kugathasan, S. The Microbiome in Patients With Inflammatory Diseases. *Clinical Gastroenterology and Hepatology* **17**, 243–255 (2019).

27. Hosomi, S., Kaser, A. & Blumberg, R. S. Role of endoplasmic reticulum stress and autophagy as interlinking pathways in the pathogenesis of inflammatory bowel disease. *Current Opinion in Gastroenterology* **31**, 81–88 (2015).

28. Bernales, S., Papa, F. R. & Walter, P. Intracellular Signaling by the Unfolded Protein Response. *Annual Review of Cell and Developmental Biology* **22**, 487–508 (2006).

29. Kaser, A. *et al.* XBP1 links ER stress to intestinal inflammation and confers genetic risk for human inflammatory bowel disease. *Cell* **134**, 743–756 (2008).

30. Zhao, F. *et al.* Disruption of Paneth and goblet cell homeostasis and increased endoplasmic reticulum stress in Agr2-/- mice. *Developmental Biology* **338**, 270–279 (2010).

31. Cadwell, K. *et al.* A key role for autophagy and the autophagy gene Atg16l1 in mouse and human intestinal Paneth cells. *Nature* **456**, 259–263 (2008).

32. Liu, B. *et al.* Irgm1-deficient mice exhibit Paneth cell abnormalities and increased susceptibility to acute intestinal inflammation. *American Journal of Physiology Gastrointestinal and Liver Physiology* **305**, G573-84 (2013).

33. Zhang, Q. *et al.* Commensal bacteria direct selective cargo sorting to promote symbiosis. *Nature Immunology* **16**, 918–926 (2015).

34. Liu, T. C. *et al.* Paneth cell defects in Crohn's disease patients promote dysbiosis. *JCI Insight* **1**, e86907 (2016).

35. Deuring, J. J. *et al.* Genomic ATG16L1 risk allele-restricted Paneth cell ER stress in quiescent Crohn's disease. *Gut* **63**, 1081–1091 (2014).

36. Hamdan, N., Kritsiligkou, P. & Grant, C. M. ER stress causes widespread protein aggregation and prion formation. *The Journal of Cell Biology* **216**, 2295–2304 (2017).

37. Tsuchiya, Y. *et al.* IRE1-XBP1 pathway regulates oxidative proinsulin folding in pancreatic β cells. *The Journal of Cell Biology* **217**, 1287–1301 (2018).

38. Cook, K. M. & Hogg, P. J. Post-Translational Control of Protein Function by Disulfide Bond Cleavage. *Antioxidant & Redox Signaling* **18**, 1987–2015 (2013).

39. Masuda, K., Sakai, N., Nakamura, K., Yoshioka, S. & Ayabe, T. Bactericidal activity of mouse α-defensin cryptdin-4 predominantly affects noncommensal bacteria. *Journal of Innate Immunity* **3**, 315–326 (2011).

40. Tanabe, H. *et al.* Denatured human alpha-defensin attenuates the bactericidal activity and the stability against enzymatic digestion. *Biochemical and Biophysical Research Communications* **358**, 349–355 (2007).

41. Rivera-Nieves, J. *et al.* Emergence of perianal fistulizing disease in the SAMP1/YitFc mouse, a spontaneous model of chronic ileitis. *Gastroenterology* **124**, 972–982 (2003).

42. Pizarro, T. T. *et al.* SAMP1/YitFc mouse strain: a spontaneous model of Crohn's disease-like ileitis. *Inflammatory Bowel Diseases* **17**, 2566–2584 (2011).

43. Cominelli, F., Arseneau, K. O., Rodriguez-Palacios, A. & Pizarro, T. T. Uncovering Pathogenic Mechanisms of Inflammatory Bowel Disease Using Mouse Models of Crohn's Disease-Like Ileitis: What is the Right Model? *Cellular and Molecular Gastroenterology and Hepatology* **4**, 19–32 (2017).

44. Rath, H. C. *et al.* Normal luminal bacteria, especially Bacteroides species, mediate chronic colitis, gastritis, and arthritis in HLA-B27/human beta2 microglobulin transgenic rats. *The Journal of Clinical Investigation* **98**, 945–953 (1996).

45. Yokoi, Y. *et al.* Paneth cell granule dynamics on secretory responses to bacterial stimuli in enteroids. *Scientific Reports* **9**, 2710 (2019).

46. Selsted, M. E. Investigational approaches for studying the structures and biological functions of myeloid antimicrobial peptides. *Genetic Engineering* **15**, 131–147 (1993).

47. Nakamura, K., Sakuragi, N. & Ayabe, T. A monoclonal antibody-based sandwich enzyme-linked immunosorbent assay for detection of secreted α-defensin. *Analytical Biochemistry* **443**, 124–131 (2013).

48. Takakuwa, A. *et al.* Butyric Acid and Leucine Induce α-Defensin Secretion from Small Intestinal Paneth Cells. *Nutrients* **11**, (2019).

49. Schägger, H. & Jagow, G. von. Tricine-sodium dodecyl sulfate-polyacrylamide gel electrophoresis for the separation of proteins in the range from 1 to 100 kDa. *Analytical Biochemistry* **166**, 368–379 (1987).

50. Herlemann, D. P. *et al.* Transitions in bacterial communities along the 2000 km salinity gradient of the Baltic Sea. *ISME Journal* **5**, 1571–1579 (2011).

51. Caporaso, J. G. *et al.* QIIME allows analysis of high-throughput community sequencing data. *Nature Methods* **7**, 335–336 (2010).

52. Edgar, R. C., Haas, B. J., Clemente, J. C., Quince, C. & Knight, R. UCHIME improves sensitivity and speed of chimera detection. *Bioinformatics* **27**, 2194–2200 (2011).

53. Edgar, R. C. Search and clustering orders of magnitude faster than BLAST. *Bioinformatics* **26**, 2460–2461 (2010).

54. Reikvam, D. H. *et al.* Depletion of murine intestinal microbiota: effects on gut mucosa and epithelial gene expression. *PLoS ONE* **6**, e17996 (2011).

55. Vidrich, A. *et al.* Altered epithelial cell lineage allocation and global expansion of the crypt epithelial stem cell population are associated with ileitis in SAMP1/YitFc mice. *The American Journal of Pathology* **166**, 1055–1067 (2005).

56. Batlle, E. *et al.* Beta-catenin and TCF mediate cell positioning in the intestinal epithelium by controlling the expression of EphB/ephrinB. *Cell* **111**, 251–263 (2002).

57. Dekaney, C. M., King, S., Sheahan, B. & Cortes, J. E. Mist1 Expression Is Required for Paneth Cell Maturation. *Cellular and Molecular Gastroenterology and Hepatology* **8**, 549–560 (2019).

58. Ouellette, A. J. *et al.* Mouse Paneth cell defensins: primary structures and antibacterial activities of numerous cryptdin isoforms. *Infection and Immunity* **62**, 5040–5047 (1994).

59. Maemoto, A. *et al.* Functional analysis of the alpha-defensin disulfide array in mouse cryptdin-4. *The Journal of Biological Chemistry* **279**, 44188–44196 (2004).

60. Walker, A. W. *et al.* High-throughput clone library analysis of the mucosa-associated microbiota reveals dysbiosis and differences between inflamed and non-inflamed regions of the intestine in inflammatory bowel disease. *BMC Microbiology* **11**, 7 (2011).

61. Manichanh, C. *et al.* Reduced diversity of faecal microbiota in Crohn's disease revealed by a metagenomic approach. *Gut* **55**, 205–211 (2006).

62. Nishino, K. *et al.* Analysis of endoscopic brush samples identified mucosa-associated dysbiosis in inflammatory bowel disease. *Journal of Gastroenterology* **53**, 95–106 (2017).

63. Frank, D. N. *et al.* Molecular-phylogenetic characterization of microbial community imbalances in human inflammatory bowel diseases. *Proceedings of the National Academy of Sciences* **104**, 13780–13785 (2007).

64. Gophna, U., Sommerfeld, K., Gophna, S., Doolittle, W. F. & Zanten, S. J. O. V. van. Differences between tissue-associated intestinal microfloras of patients with Crohn's disease and ulcerative colitis. *Journal of Clinical Microbiology* **44**, 4136–4141 (2006).

65. Marini, M. *et al.* TNF-alpha neutralization ameliorates the severity of murine Crohn's-like ileitis by abrogation of intestinal epithelial cell apoptosis. *Proceedings of the National Academy of Sciences* **100**, 8366–8371 (2003).

66. Odashima, M. *et al.* Activation of A2A Adenosine Receptor Attenuates Intestinal Inflammation in Animal Models of Inflammatory Bowel Disease. *Gastroenterology* **129**, 26–33 (2005).

67. Million, M. *et al.* New insights in gut microbiota and mucosal immunity of the small intestine. *Human Microbiome Journal* **7–8**, 23–32 (2018).

68. Wexler, H. M. Bacteroides: the good, the bad, and the nitty-gritty. *Clinical Microbiology Reviews* **20**, 593–621 (2007).

69. Walker, A. *et al.* Sulfonolipids as novel metabolite markers of Alistipes and Odoribacter affected by high-fat diets. *Scientific Reports* **7**, 1–10 (2017).

70. Ferguson, L. R., Laing, B., Marlow, G. & Bishop, K. The role of vitamin D in reducing gastrointestinal disease risk and assessment of individual dietary intake needs: Focus on genetic and genomic technologies. *Molecular Nutrition & Food Research* **60**, 119–133 (2015).

71. Gombart, A. F., Borregaard, N. & Koeffler, H. P. Human cathelicidin antimicrobial peptide (CAMP) gene is a direct target of the vitamin D receptor and is strongly up-regulated in myeloid cells by 1,25-dihydroxyvitamin D3. *FASEB Journal* **19**, 1067–1077 (2005).

72. Su, D. *et al.* Vitamin D Signaling through Induction of Paneth Cell Defensins Maintains Gut Microbiota and Improves Metabolic Disorders and Hepatic Steatosis in Animal Models. *Frontiers in Physiology* **7**, 471–18 (2016).

73. Wu, S. *et al.* Intestinal epithelial vitamin D receptor deletion leads to defective autophagy in colitis. *Gut* **64**, 1082–1094 (2015).

74. VanDussen, K. L. *et al.* Genetic variants synthesize to produce Paneth cell phenotypes that define subtypes of Crohn's disease. *Gastroenterology* **146**, 200–209 (2014).

75. Wehkamp, J. *et al.* NOD2 (CARD15) mutations in Crohn's disease are associated with diminished mucosal alpha-defensin expression. *Gut* **53**, 1658–1664 (2004).

76. Williams, A. D. *et al.* Human alpha defensin 5 is a candidate biomarker to delineate inflammatory bowel disease. *PLoS ONE* **12**, e0179710 (2017).

77. Ananthakrishnan, A. N. *et al.* Zinc intake and risk of Crohn's disease and ulcerative colitis: a prospective cohort study. *International Journal of Epidemiology* **44**, 1995–2005 (2015).

78. Guo, X. *et al.* Rutin and Its Combination With Inulin Attenuate Gut Dysbiosis, the Inflammatory Status and Endoplasmic Reticulum Stress in Paneth Cells of Obese Mice Induced by High-Fat Diet. *Frontiers in Microbiology* **9**, 2651 (2018).

79. Podany, A. B., Wright, J., Lamendella, R., Soybel, D. I. & Kelleher, S. L. ZnT2-Mediated Zinc Import Into Paneth Cell Granules Is Necessary for Coordinated Secretion and Paneth Cell Function in Mice. *Cellular and Molecular Gastroenterology and Hepatology* **2**, 369–383 (2016).

80. Hess, D. A. *et al.* MIST1 Links Secretion and Stress as both Target and Regulator of the Unfolded Protein Response. *Molecular and Cell Biology* **36**, 2931–2944 (2016).

81. Pin, C. L., Rukstalis, J. M., Johnson, C. & Konieczny, S. F. The bHLH transcription factor Mist1 is required to maintain exocrine pancreas cell organization and acinar cell identity. *Journal of Cell Biology* **155**, 519–530 (2001).

82. Jing, W., Hunter, H. N., Tanabe, H., Ouellette, A. J. & Vogel, H. J. Solution structure of cryptdin-4, a mouse Paneth cell α-defensin. *Biochemistry* **43**, 15759–15766 (2004).

83. Szyk, A. *et al.* Crystal structures of human alpha-defensins HNP4, HD5, and HD6. *Protein Science* **15**, 2749–2760 (2006).

84. Hadjicharalambous, C. *et al.* Mechanisms of alpha-defensin bactericidal action: comparative membrane disruption by Cryptdin-4 and its disulfide-null analogue. *Biochemistry* **47**, 12626–12634 (2008).

85. Zhang, Y., Cougnon, F. B. L., Wanniarachchi, Y. A., Hayden, J. A. & Nolan, E. M. Reduction of human defensin 5 affords a high-affinity zinc-chelating peptide. *ACS chemical biology* **8**, 1907–1911 (2013).

86. Meyers, S. *et al.* Fecal alpha 1-antitrypsin measurement: an indicator of Crohn's disease activity. *Gastroenterology* **89**, 13–18 (1985).

87. Wanniarachchi, Y. A., Kaczmarek, P., Wan, A. & Nolan, E. M. Human defensin 5 disulfide array mutants: disulfide bond deletion attenuates antibacterial activity against Staphylococcus aureus. *Biochemistry* **50**, 8005–8017 (2011).

88. Schroeder, B. O. *et al.* Paneth cell α-defensin 6 (HD-6) is an antimicrobial peptide. *Mucosal Immunology* **8**, 661–671 (2015).

89. Wang, C. *et al.* Reduction Impairs the Antibacterial Activity but Benefits the LPS Neutralization Ability of Human Enteric Defensin 5. *Scientific Reports* **6**, 22875 (2016).

90. Hodin, C. M. *et al.* Reduced Paneth cell antimicrobial protein levels correlate with activation of the unfolded protein response in the gut of obese individuals. *The Journal of pathology* **225**, 276–284 (2011).

91. Grootjans, J. *et al.* Level of activation of the unfolded protein response correlates with Paneth cell apoptosis in human small intestine exposed to ischemia/reperfusion. *Gastroenterology* **140**, 529-539.e3 (2011).

92. Gyongyosi, B. *et al.* Alcohol-induced IL-17A production in Paneth cells amplifies endoplasmic reticulum stress, apoptosis, and inflammasome-IL-18 activation in the proximal small intestine in mice. *Mucosal Immunology* **12**, 930–944 (2019)

7. Figures

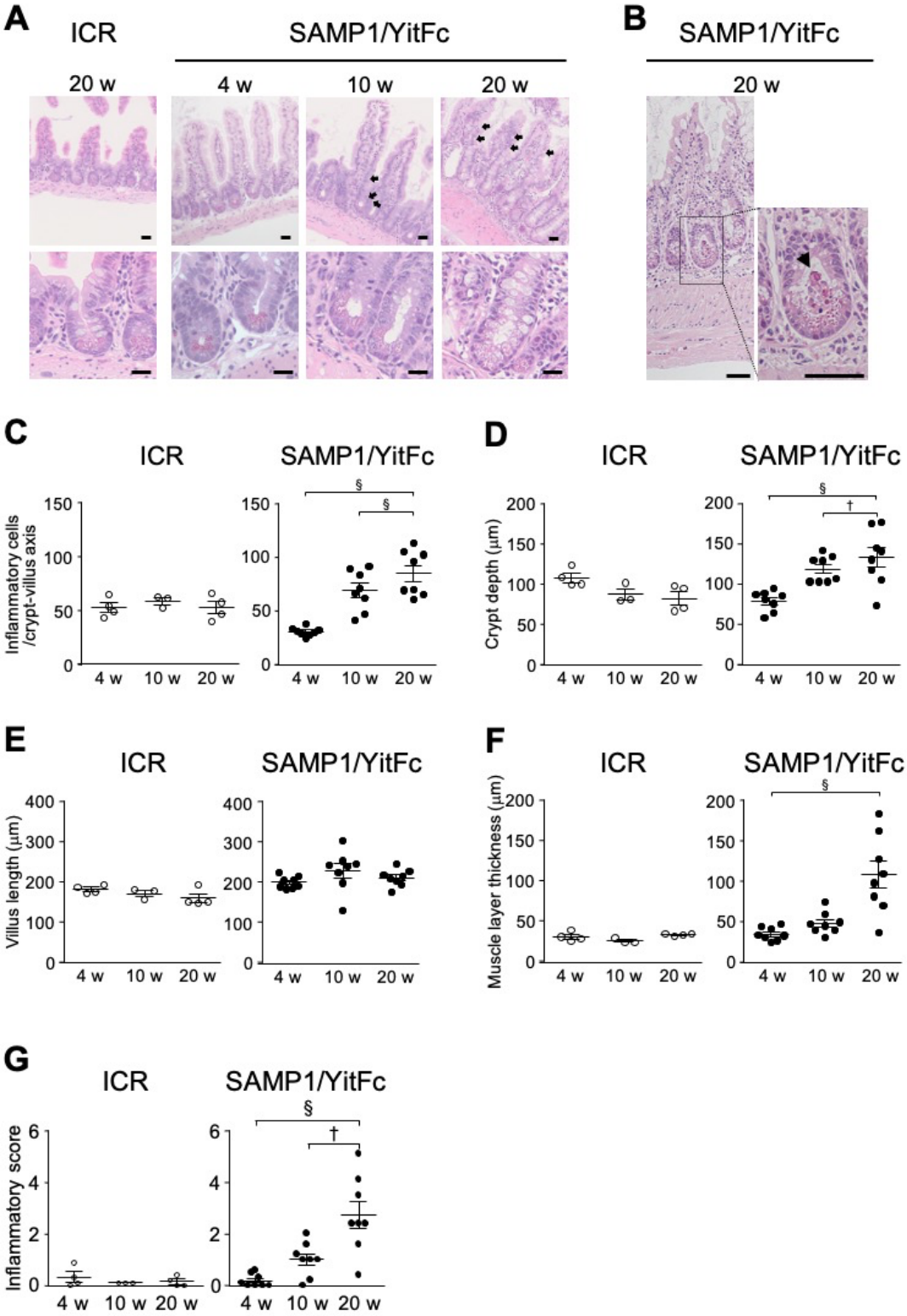
A
ICR
SAMP1/YitFc
20 w
4 w
10 w
20 w
B
SAMP1/YitFc
20 w
C
ICR
SAMP1/YitFc
Inflammatory cells /crypt-villus axis
150
100
50
0
4 w
10 w
20 w
§
§
D
ICR
SAMP1/YitFc
Crypt depth (μm)
200
150
100
50
0
§
†
E
ICR
SAMP1/YitFc
Villus length (μm)
400
300
200
100
0
F
ICR
SAMP1/YitFc
Muscle layer thickness (μm)
§
G
ICR
SAMP1/YitFc
Inflammatory score
6
4
2
0
§
†

Figure 1. Disease progression in SAMP1/YitFc mice

(A) Representative HE staining images of ileal tissues. Abnormal Paneth cells in upper crypts and on villi are indicated by black arrows. **(B)** Representative HE images of crypt abscess. **(C)** Number of inflammatory cells, an index of inflammatory infiltration (n = 3-4/week in ICR mice, n = 8/week in SAMP1/YitFc mice). **(D)** Crypt depth and **(E)** villus length, indexes of crypt elongation. **(F)** Muscle layer thickness, an index of thickening of muscle layer. **(G)** Total inflammatory score. In (A, B), scale bars indicate 20 μm. In (C-G), error bars indicate mean ± SEM., and statistical significance was evaluated by one-way ANOVA followed by Tukey's post hoc test. †: $p < 0.01$, §: $p < 0.001$

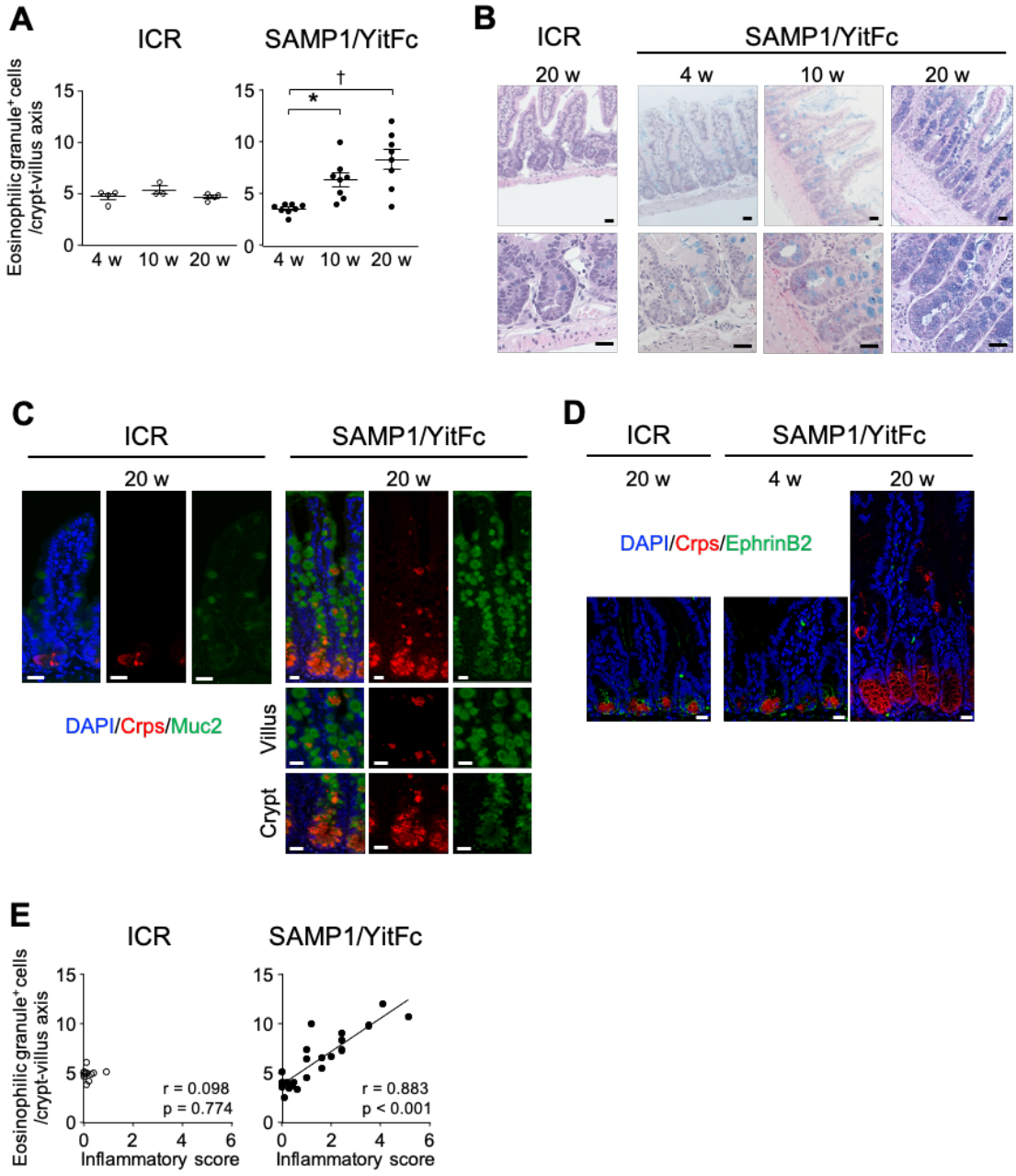
A
ICR
SAMP1/YitFc
Eosinophilic granule+ cells /crypt-villus axis
15
10
5
0
4 w
10 w
20 w
*
†
B
ICR
SAMP1/YitFc
20 w
4 w
10 w
20 w
C
ICR
SAMP1/YitFc
20 w
20 w
DAPI/Crps/Muc2
Villus
Crypt
D
ICR
SAMP1/YitFc
20 w
4 w
20 w
DAPI/Crps/EphrinB2
E
ICR
SAMP1/YitFc
Eosinophilic granule+ cells /crypt-villus axis
r = 0.098
p = 0.774
r = 0.883
p < 0.001
Inflammatory score
Inflammatory score

Figure 2. Increase of abnormal Paneth cells during disease progression

(A) Number of eosinophilic granule^{+} cells (n = 3-4/week in ICR mice, n = 8/week in SAMP1/YitFc mice). **(B)** Representative HE-alcian blue staining images of ileal tissues. **(C)** Representative immunofluorescent staining images for Muc2 (green), Crps (Red), and DAPI (blue) in ileal tissues. **(D)** Representative immunofluorescent staining images for EphrinB2 (green), Crps (Red), and DAPI (blue) in ileal tissues. **(E)** Correlation analysis between the number of eosinophilic granule $^{+}$ cells and inflammatory scores in each mouse at 4, 10, 20 w. In (A), error bars indicate mean ± SEM. In (B-D), scare bars indicate 20 μm. Statistical significance was evaluated by one-way ANOVA followed by Tukey's post hoc test in (A) and Pearson's correlation coefficients test in (E). *: $p < 0.05$, †: $p < 0.01$.

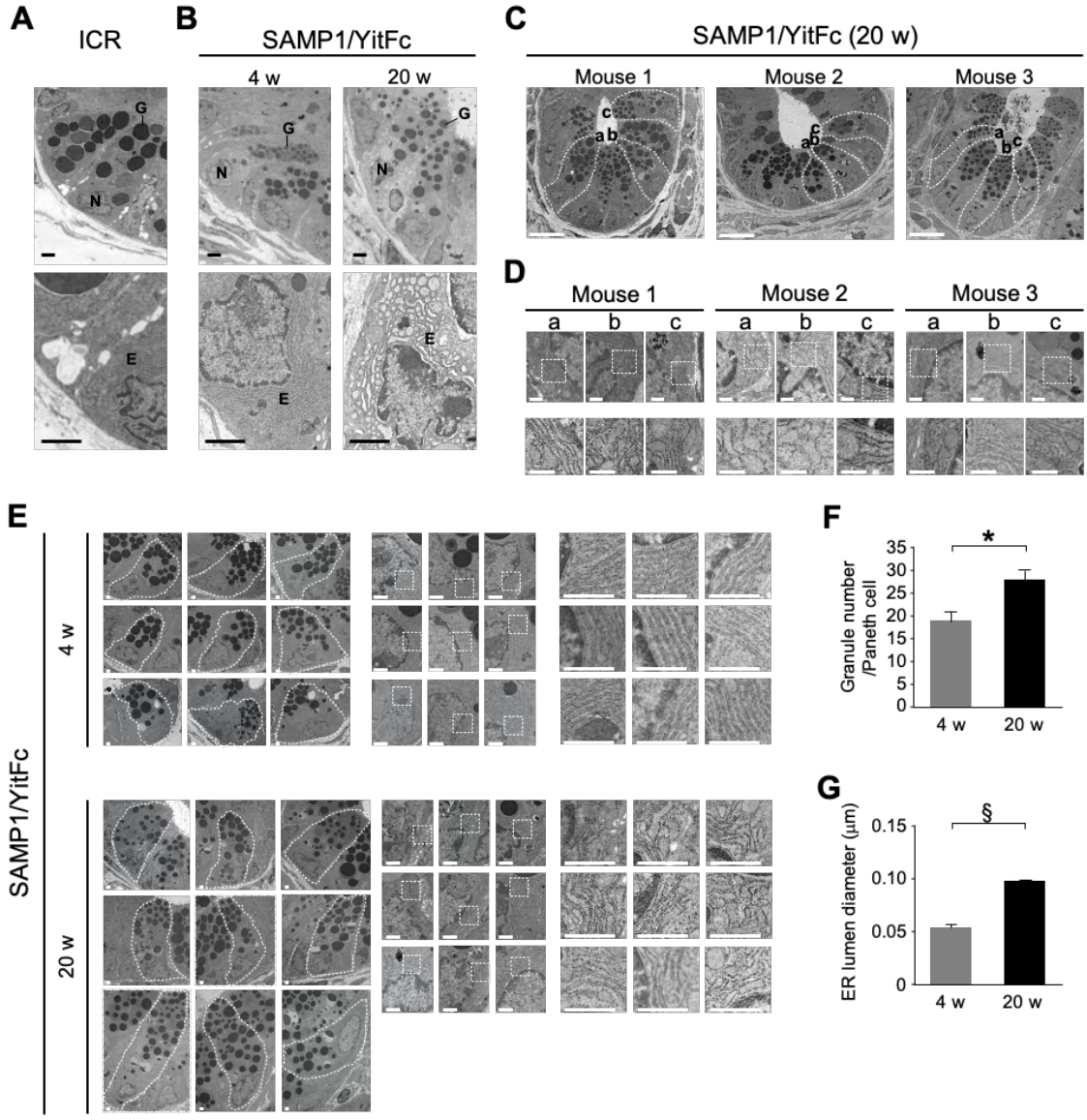
A
ICR
B
SAMP1/YitFc
4 w
20 w
C
SAMP1/YitFc (20 w)
Mouse 1
Mouse 2
Mouse 3
D
Mouse 1
Mouse 2
Mouse 3
a
b
c
E
SAMP1/YitFc
4 w
20 w
F
Granule number /Paneth cell
35
30
25
20
15
10
5
0
*
4 w
20 w
G
ER lumen diameter (μm)
0.15
0.10
0.05
0
§
4 w
20 w

Figure 3. Structural disorders in intracellular organelles of abnormal Paneth cells

(A, B) Representative transmission electron microscopy (TEM) images of Paneth cells at the base of ileal crypts in (A) ICR and (B) SAMP1/YitFc mice. G, granules, N, nucleus, E, ER. Scale bars indicate 2 μm. **(C)** Representative TEM images of ileal crypts in 20 w SAMP1/YitFc mice obtained from 3 individual mice. Scale bars indicate 10 μm. **(D)** High-magnification images of ER in randomly selected 3 Paneth cells (a, b, c) from each crypt. Scale bars indicate 500 nm. **(E)** Representative TEM images of Paneth cells at the base of ileal crypts in SAMP1/YitFc mice used for quantitative analyses. Scale bars indicate 1 μm. (E, F) Quantitative analysis of (E) granule number and (F) ER lumen diameter in Paneth cells of SAMP1/YitFc mice (n = 3/week). In (E, F), error bars indicate mean ± SEM, and statistical significance was evaluated by unpaired Student's T test. *: $p < 0.05$, †: $p < 0.01$.

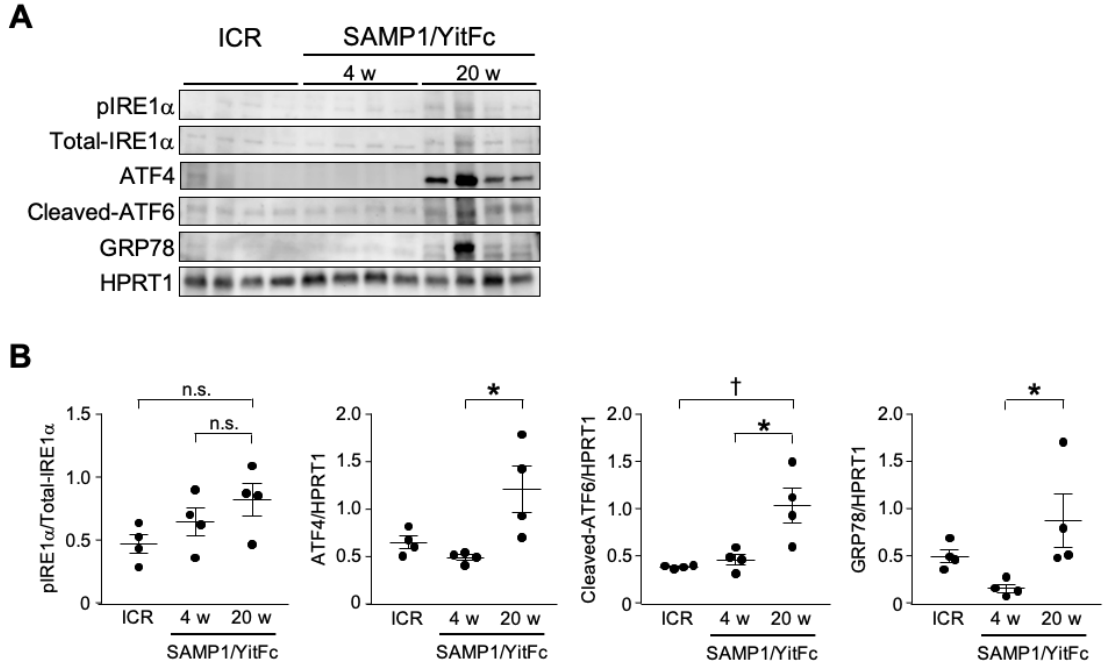

Figure 4. Increase of ER stress marker expression in isolated ileal crypts

(A) SDS-PAGE western blot analysis of ER stress markers, pIRE1α, ATF4, cleaved-ATF6 and GRP78 in ileal crypts isolated from 12-15 w ICR mice, 4 and 20 w SAMP1/YitFc mice (n = 4/each group). Total-IRE1α and HPRT1 was used as loading control. **(B)** Relative expression level of ER stress markers calculated from the band intensity. In (B), error bars indicate mean ± SEM., and statistical significance was evaluated by one-way ANOVA followed by Tukey post hoc test. n.s., not significant, *, $p < 0.05$, †, $p < 0.01$.

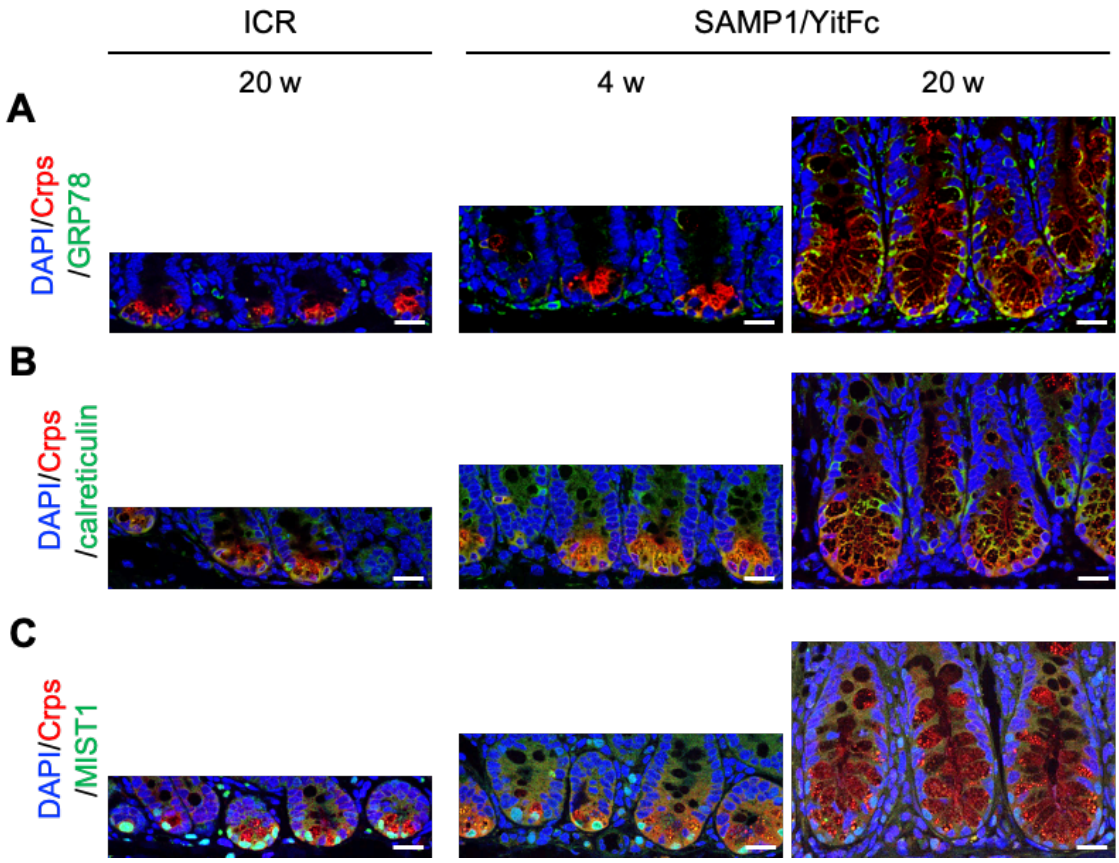

Figure 5. Aberrant expression profiles of ER stress-related proteins in abnormal Paneth cells

(A) Representative immunofluorescent staining images for GRP78 (green), Crps (Red), and DAPI (blue) in ileal tissues. **(B)** Representative immunofluorescent staining images for calreticulin (green), Crps (Red), and DAPI (blue) in ileal tissues. **(C)** Representative immunofluorescent staining images for MIST1 (green), Crps (Red), and DAPI (blue) in ileal tissues. Scare bars indicate 20 μm.

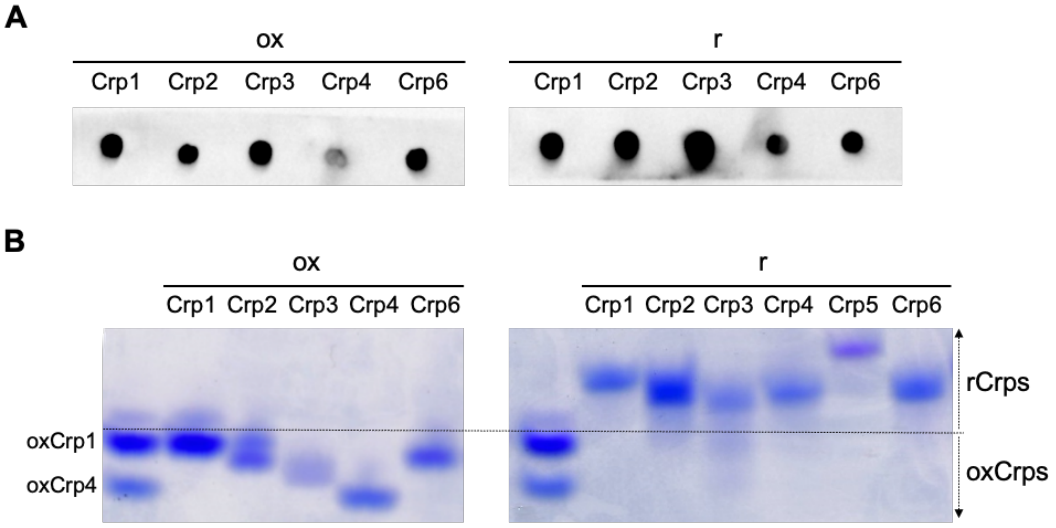

Figure 6. Immunoreactivities and electrophoretic mobilities of Crp isoforms

(A) To confirm whether anti-Crp1 antibody used in this study can react with both oxidized-form (ox) and reduced-form (r) of multiple Crp isoforms, immunoreactivities against Crp isoforms was determined by dot blot analysis using 50 ng of chemically synthesized ox and rCrp1–6. The antibody reacted with Crp1–4 and 6 of both ox and rCrp isoforms. Thus, we confirmed that the antibody is pan-Crp antibody which can detect both ox and rCrps. **(B)** Mobilities of each rCrp and oxCrp isoform in the AU-PAGE system as visualized by Coomassie Brilliant Blue staining using 500 ng of chemically synthesized ox and rCrp1.

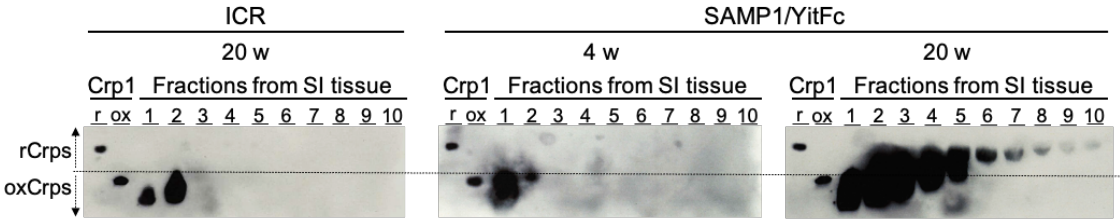

Figure 7. Accumulation of reduced-form α-defensin in abnormal Paneth cells

Protein was extracted from full length of small intestinal (SI) tissue obtained from ten ICR and ten SAMP1/YitFc mice and fractionated by using preparative acid native-PAGE system. AU-PAGE western blot analysis of Crps in each fraction was conducted. Fraction numbers denote the order of elution during fractionation. 200 ng of chemically synthesized ox and rCrp1 were used as markers for identifying the conformation of Crps in each fraction. Based on band motility, Crps detected in the mobility zone below oxCrp1 (below the dotted line) was judged as oxCrps, and Crps detected in the lower motility zone than that of oxCrp1 (above the dotted line) was judged as rCrps.

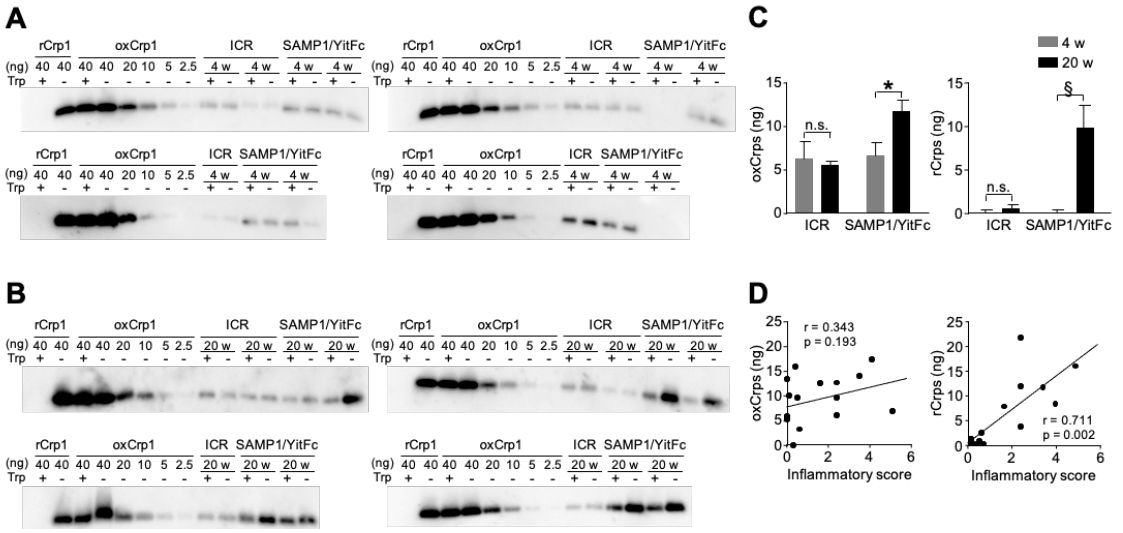

Figure 8. Secretion of reduced-form α-defensin into the intestinal lumen during the disease progression

(A, B) Tricine SDS-PAGE western blot analysis of Crps in fecal extracts of (A) 4 w and (B) 20 w (ICR mice; n = 6, SAMP1/YitFc mice; n = 8/week). Chemically synthesized ox and rCrp1 were used as positive controls. Each sample was treated with trypsin (Trp+) or PBS (Trp-). **(C)** The amount of ox and rCrps in fecal extracts. The amount of oxCrps in each sample was calculated from band intensity of Trp+, and the amount of rCrps was calculated from the difference between band intensity of Trp- and Trp+. **(D)** Correlation analysis between the quantity of fecal Crps and inflammatory scores of each SAMP1/YitFc mouse. Error bars represent mean ± SEM. Statistical significance was evaluated by Mann-Whitney's U test in (C), and by Pearson's correlation coefficients test in (D). *, $p < 0.05$, §, $p < 0.001$.

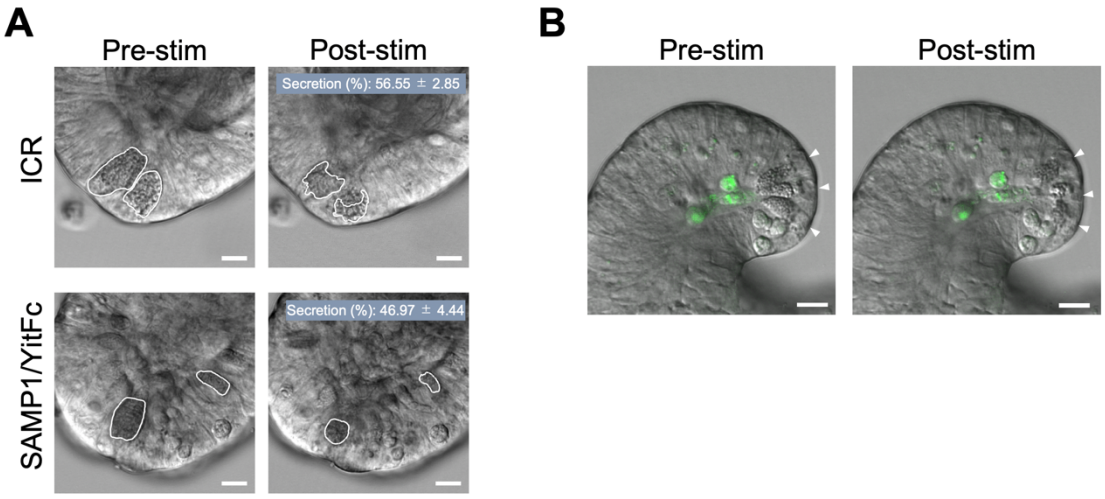

Figure 9. Granule secretion of abnormal Paneth cells in SAMP1/YitFc mouse enteroids

(A) Representative differential interference contrast images of Paneth cells in enteroids from ICR and SAMP1/YitFc mice pre- and post-stimulation of 10 μM CCh. Granule secretion (%) were indicated as mean ± SEM. and showed no significant difference between ICR mouse and SAMP1/YitFc mouse enteroids ($p = 0.231$). **(B)** Representative still images from time-lapse analysis for caspase-3/7 activity of Paneth cells (white arrow heads) in SAMP1/YitFc mouse enteroids stimulated by 10 μM CCh. In (A-B), scale bars indicate 10 μm. In (A), statistical significance was evaluated by Mann-Whitney's U test. $p < 0.05$ was considered statistically significant.

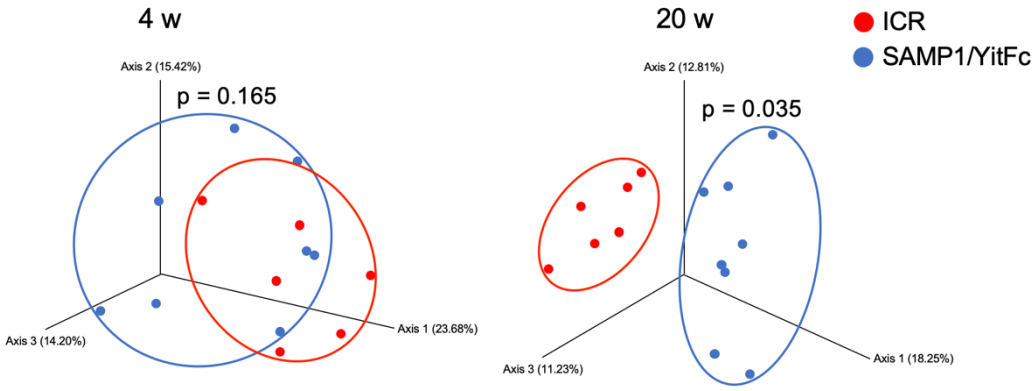

Figure 10. Shift of microbial structure between ICR and SAMP1/YitFc mice during disease progression

Comparison of β-diversity between ICR mouse and SAMP1/YitFc mouse intestinal microbiota at 4 and 20 w by PCoA plot based on unweighted UniFrac distance. Statistical significance was evaluated by PERMANOVA test. $p < 0.05$ was considered statistically significant.

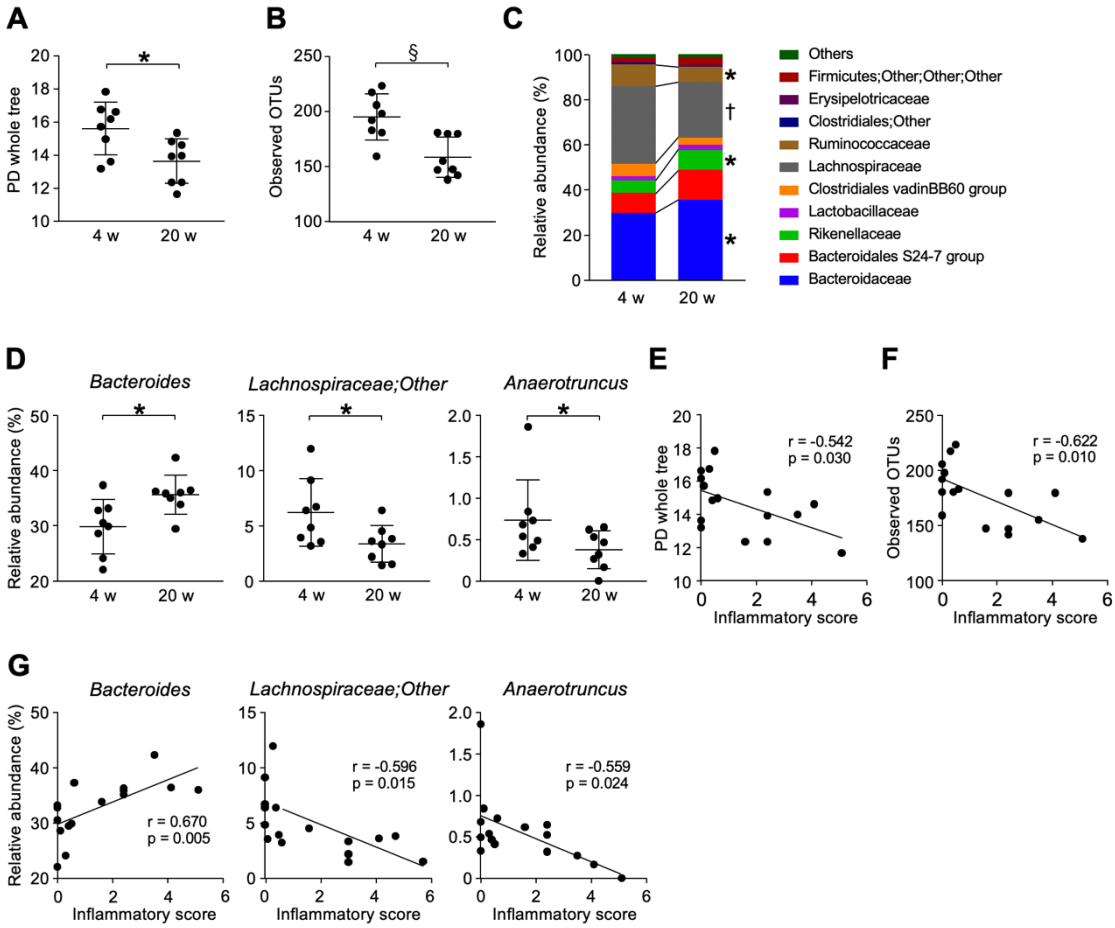

Figure 11. Dysbiosis along with disease progression

(A, B) Two α-diversity indexes, (A) PD whole tree and (B) observed OTUs in SAMP1/YitFc mice. **(C)** Stacked bar chart of relative abundance of each taxon in SAMP1/YitFc mice at the family level. **(D)** Dot plots of significantly changed taxa in SAMP1/YitFc mice at genus levels. **(E-G)** Correlation analysis between inflammatory scores and (E, F) α-diversify indexes or (G) significantly changed genus in each SAMP1/YitFc mouse. In (A, B, D), error bars indicate mean ± SEM. Statistical significance was evaluated by Mann-Whitney's U test in (A–D), and Pearson's correlation coefficients test in (E–G). *, $p < 0.05$, †, $p < 0.01$, §, $p < 0.001$.

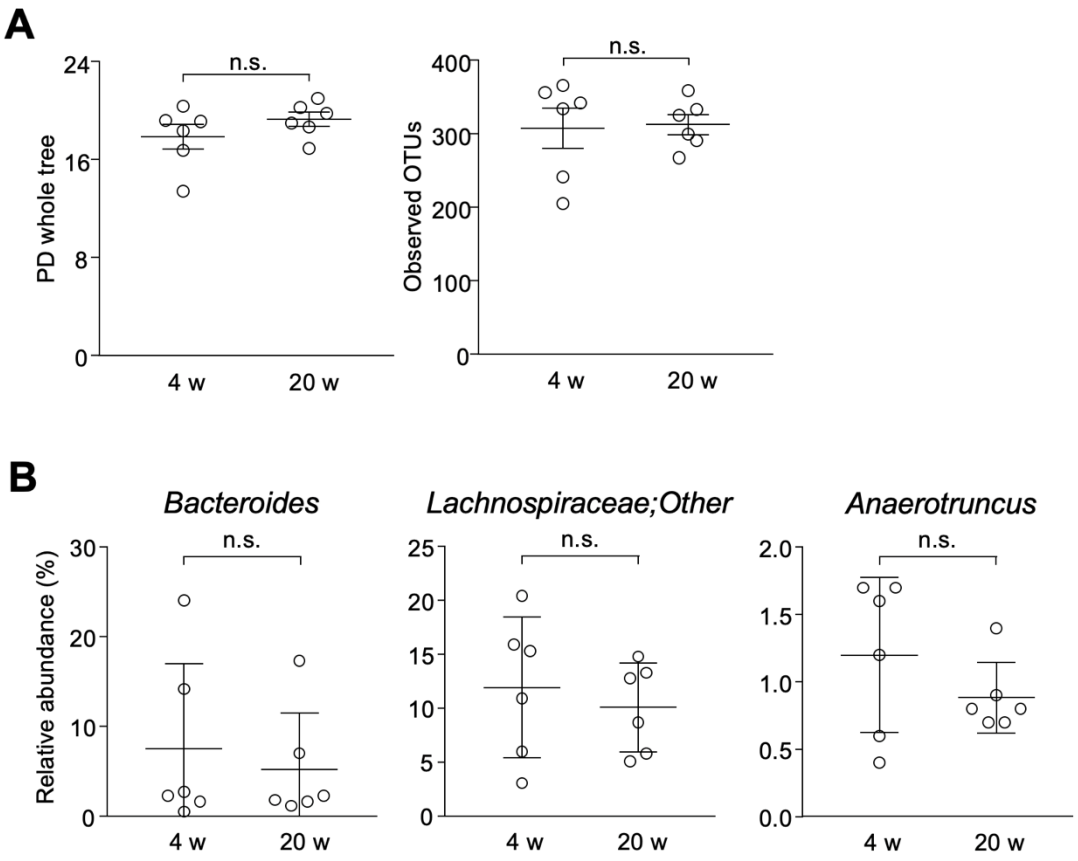

Figure 12. Analysis of α-diversity and ileitis-related bacteria along with age in week of ICR mice

(A) Two α−diversity indexes, PD whole tree and observed OTUs in 4 and 20 w ICR mice (n = 6/week). **(B)** Relative abundance of *Bacteroides*, *Lachnospiraceae;Other*, and *Anaerotruncus* which are significantly changed genus in SAMP1/YitFc mice during pathological progression, in 4 and 20 w ICR mice. Error bars represent mean ± SEM. Statistical significance was evaluated by Mann-Whitney's U test. n.s., not significant.

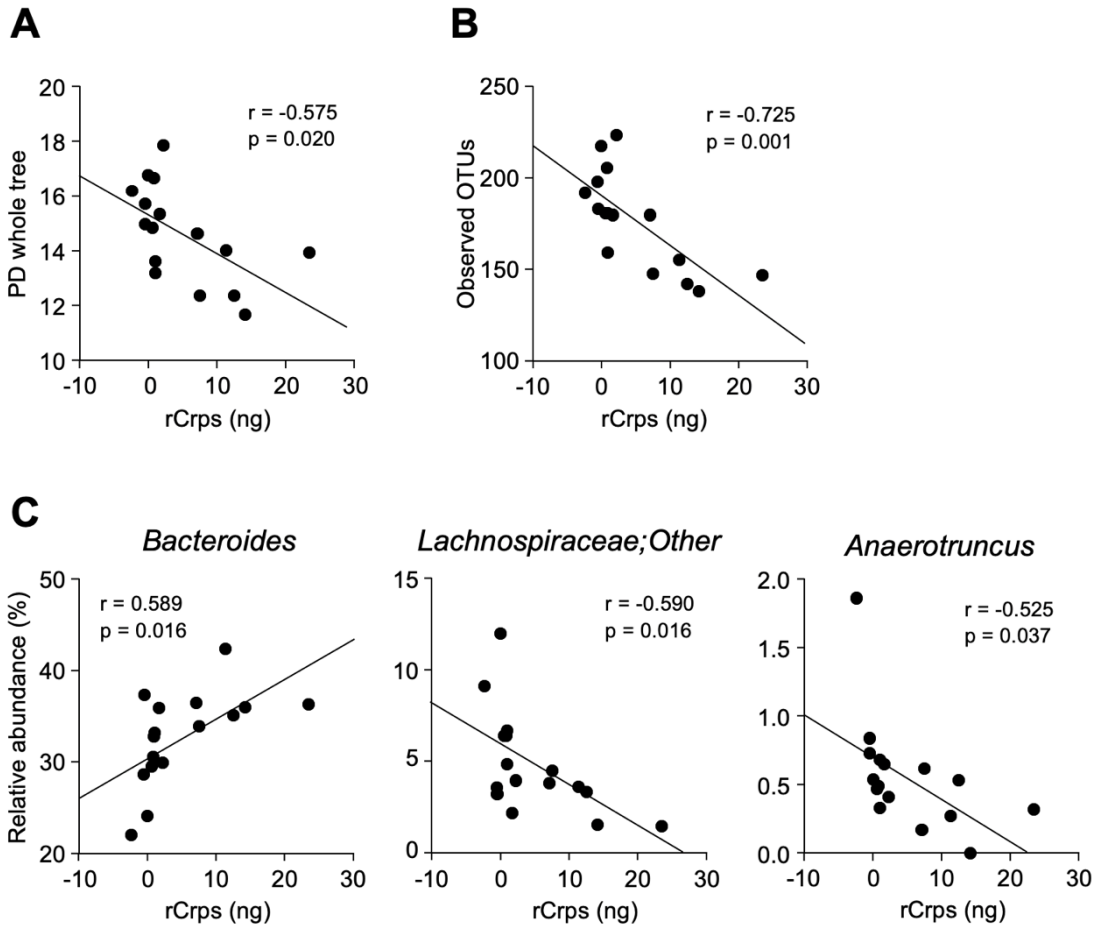

Figure 13. Involvement of reduced-form α-defensin secretion in dysbiosis during disease progression

(A, B) Correlation analysis between the amount of fecal rCrps and α-diversity indexes of each SAMP1/YitFc mouse. **(C)** Correlation analysis between the quantity of fecal rCrps and relative abundance of significantly changed taxa in SAMP1/YitFc mice. Statistical significance was evaluated by Pearson's correlation coefficients test. $p < 0.05$ was considered statistically significant.

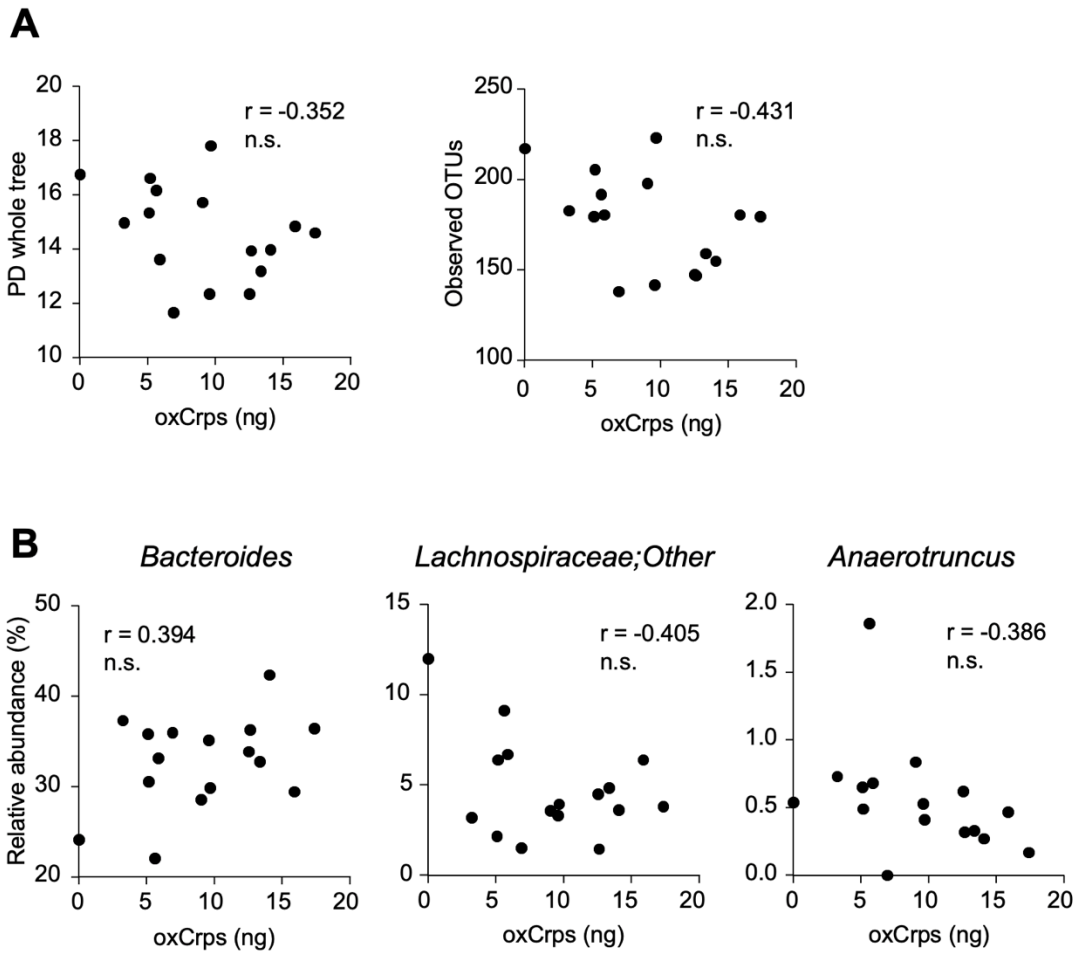

Figure 14. Correlation analysis between secretion of oxidized-form Crps into feces and dysbiosis during the disease progression.

(A, B) Correlation analysis between the amount of fecal oxCrps and α-diversity indexes of each SAMP1/YitFc mouse. **(C)** Correlation analysis between the quantity of fecal oxCrps and relative abundance of significantly changed taxa in SAMP1/YitFc mice. Statistical significance was evaluated by Pearson's correlation coefficients test. n.s., not significant.

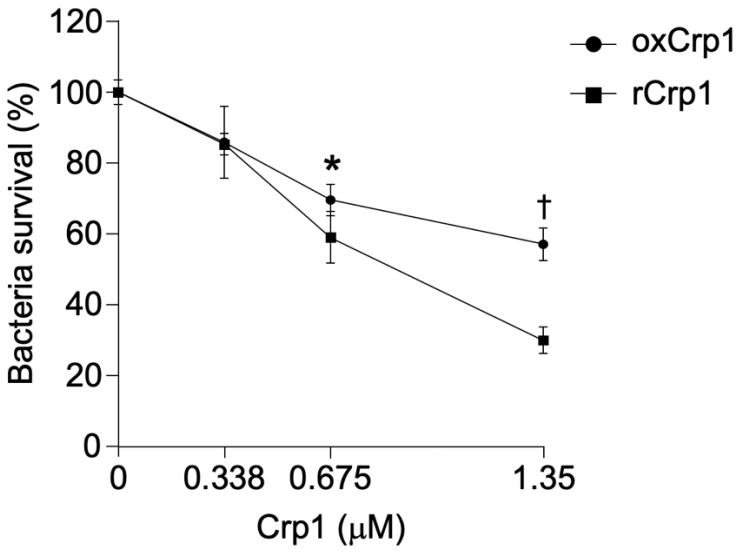

Figure 15. Comparison of *in vitro* bactericidal activities of oxidized-form Crp1 and reduced-form Crp1 against *Anaerotruncus coliholminis*

Bactericidal activity of ox and rCrp1 against *Anaerotruncus coliholminis*, a commensal bacterium decreased in SAMP1/YitFc mice during disease progression, was analyzed *in vitro* (n = 5 at each concentration). Error bars represent mean ± SEM. Statistical significance was evaluated by two-way ANOVA followed by Mann-Whitney's U test. *, $p < 0.05$, †, $p < 0.01$.

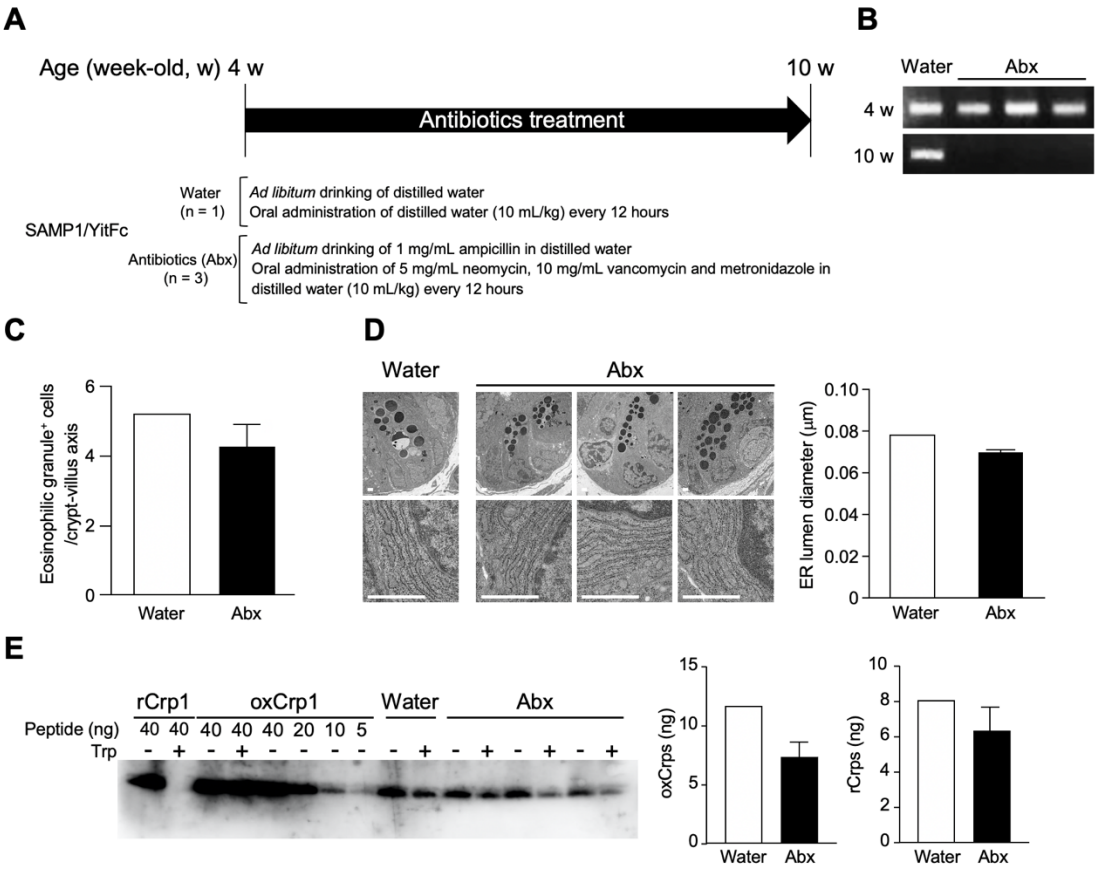

Figure 16. Paneth cell abnormalities after depletion of the intestinal microbiota by antibiotics treatment in SAMP1/YitFc mice

(A) Scheme of experimental procedures. **(B)** PCR products of microbial 16S rDNA in feces. **(C)** Numbers of eosinophilic granule-positive cells. **(D)** Representative TEM image of Paneth cell and measurement of ER lumen diameter. For the measurement, 6 Paneth cells were randomly selected from each mouse. **(E)** Quantification of ox and rCrps. In (C−E), Error bars represent mean ± SEM.

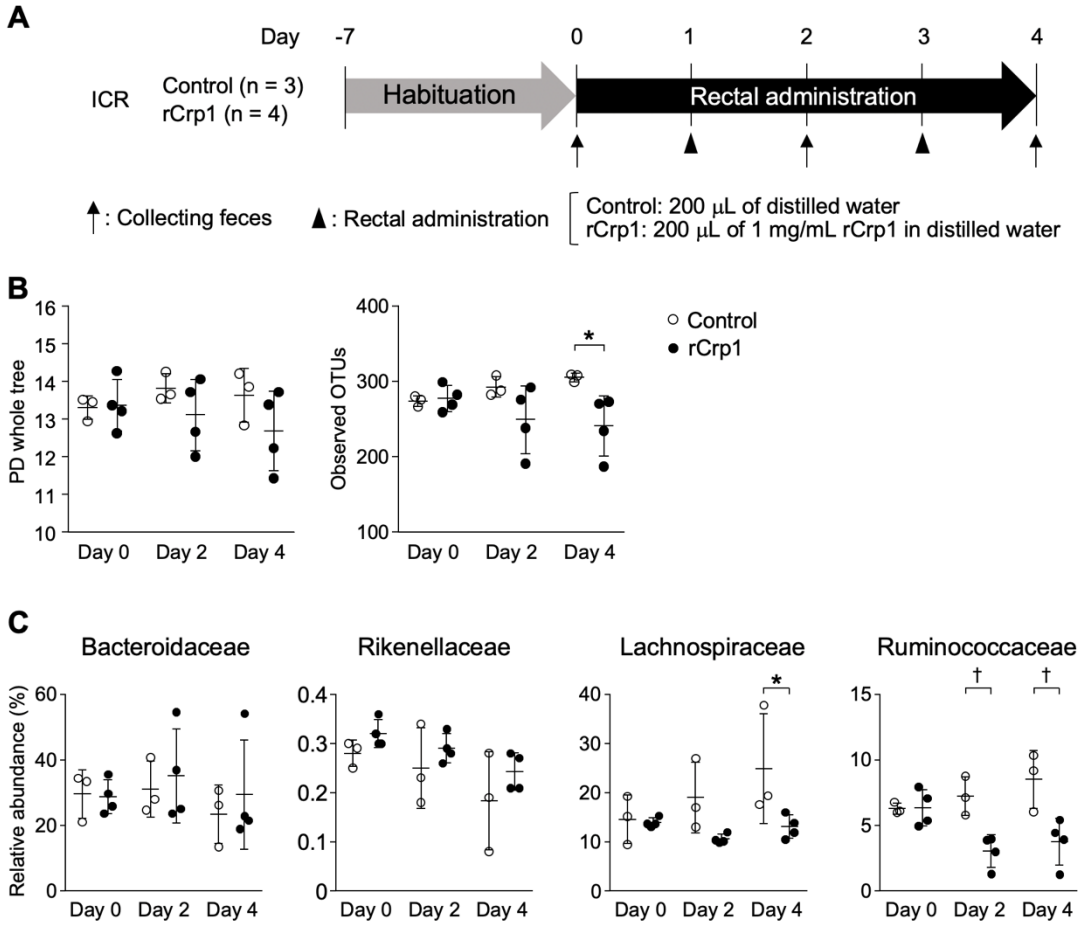

Figure 17. Intestinal microbiota modulation by rectal administration of reduced-form Crp1 to ICR mice

(A) Scheme of experimental procedures. **(B)** Comparison of α-diversity indices. **(C)** Comparison of relative abundance of bacteria that significantly shifted in SAMP1/YitFc mice during disease progression at the family level. Error bars represent mean ± S.E.M. Statistical significance was evaluated by two-way ANOVA followed by Bonferroni post hoc test in (B) and (C). $p < 0.05$ was considered statistically significant. *, $p < 0.05$, †, $p < 0.01$

Table 1. Criteria for evaluating inflammatory score

Evaluation item	Score	Grade
[a] Inflammatory infiltration	0	≦ 81 cells
(The number of inflammatory cells)	1	82–116 cells
	2	117–151 cells
	3	152 cells ≦
[b] Villus distortion	0	1.5 <
(Villus length / crypt depth)	1	1.0–1.5
	2	0.5–1.0
	3	< 0.5
[c] Thickening of muscle layer	0	≦ 45 μm
(Thickness of muscle layer)	1	46–114 μm
	2	115–183 μm
	3	184 μm ≦
[d] Number of crypt abscesses	0.5 x number	

8. Acknowledgements

First, I would like to express my deep gratitude to all the people who supported me for the accomplishment of this work. My supervisor, Professor Tokiyoshi Ayabe gives me considerable supports in all aspects of my laboratory life. I could keep going my doctoral study with his sincere encouragement and excellent guidance. Associate Professor Kiminori Nakamura directly instructed me throughout the research. I always learn about the attitude toward research from him. Professor Tomoyasu Aizawa had acted as an associate examiner from my master's course and continuously supports my research. Professor Andre J Ouellette at Kech School of Medicine in University of Southern California gives me lots of constructive advices through helpful discussion. I received generous supports from Dr. Naoya Sakuragi, Dr. Mani Kikuchi, and Dr. Yuki Yokoi for the procedure of the experiments in this study. Ms. Aiko Kuroishi and Ms. Mutsuko Tanaka gives me enormous technical supports. Ms. Mari Tatsumi always helps my laboratory activities. Finally, I want to thank all laboratory members for continuing support for my laboratory life.